

Characteristics of the amphibolite rocks of Penjween area, Kurdistan Region, northeast Iraq: Genetic implication and association with Penjween Ophiolite Complexes

Ayten Hadi^{1*} Dalya Kameran² Sabah Ismael²

Department of Earth Science, College of Science – University of Baghdad .1

Department of Applied Geology, College of Science – University of Kirkuk .2

* E-mail of the corresponding author: ayten_alshareefy@yahoo.com

Abstract

Amphibolite rocks are found in Penjween ophiolite complexes within the Iraqi Zagros Thrust Zone, northeast Iraq. They appear in a discontinuous outcrops as pods and lenses in a sharp contact with peridotite and serpentinite rocks. Amphibole and plagioclase are the main mineral constituents with minor amount of clinopyroxene and quartz, Fe-Ti-oxides, titanite, apatite, zircon as accessory phases. Two mineral assemblages are recognized in these amphibolites; (1) amphibole+ plagioclase+ clinopyroxene+ iron oxides +titanite ± quartz± apatite± zircon; (2) amphibole+ plagioclase +iron oxide+ titanite± quartz± apatite± zircon, with chlorite, epidote and actinolite as secondary mineral phases. These amphibolites show different textures as granoblastic, granonematoblastic, porphyroblastic, and poikiloblastic. The amphiboles are calcic ($Ca > 1$ apuf) and are of two types; Mg- hornblende and tschermakite. They are characterized by: SiO_2 (38.83-47.48%), Al_2O_3 (7.97-16.02%), TiO_2 (0.28-3.04%), MgO (12.03-16.38%), CaO (11.01-12.46%), FeO (8.55-13.4%) and Mg^* (0.62-0.76). Plagioclase composition ranges between oligoclase ($An_{23.4}-Ab_{75.9}$) and albite ($An_{1.7}-Ab_{97.9}$). Geothermobarometry based on $TiO_2-Al_2O_3$ isopleths of calcic amphibole show that both Mg-hornblende and tschermakite have P range (1.5-2.5 GPa) and T range (550-700°C) for Mg-hornblende and (700-900°C) for tschermakite, which are within amphibolite facies grade. Geochemical characteristics of these amphibolites indicate their igneous origin of tholeiitic basalt affinity with sub-alkaline basalt and andesite protoliths that are formed by fractionation of clinopyroxene, plagioclase and Fe-Ti- oxides. Primitive mantle- normalized trace elements diagram show similarity with subduction zone setting with striking variable enrichment of LILE, depletion of HFSE and HREE, and negative Nb-Ta anomalies. Chondrite normalized-REE diagram show LREE enrichment $(La/Sm)_N = 3.295$, $(La/Yb)_N = 3.919$ indicating the existence of garnet as residual phase in the source mantle. Tectonic discrimination diagrams based on immobile elements suggest island arc tholeiite, specifically back-arc basin basalt setting with 5-25% partial melting. The negative Nb-Ta anomalies, high Th and Ba/Yb, and $La/Nb < 5$, all confirm the back-arc basin setting or supra-subduction zone environment. This is consistent with the proposed idea that these amphibolites are genetically related to Penjween ophiolite and represent oceanic crustal rocks and sea-floor sediments that were detached and emplaced by mantle rocks of the ophiolite onto the Arabian Plate margin during Late Cretaceous. The processes of detachment and emplacement cause metamorphism of the oceanic crustal rocks reaching amphibolite facies grade.

Key words: Amphibolite, Penjween ophiolite, SSZ

1. Introduction

The Iraqi Zagros Thrust Zone (IZTZ) represents the suture zone between the Arabian and Iranian Plates. This zone extends in a northwest-southeast direction from the Turkish-Iranian border as a result of the collision between the Arabian and Eurasian Plates which occurred during Cenozoic Time (Stöckline, 1968, Alavi, 1994, 2004). It is considered as a part of Zagros Orogenic Belt which extends for about 2000 km. from southeast Turkey through Syria and Iraq to the western and southern Iran and is considered an integral part of the main Alpine- Himalayan Orogenic Belt (Ricou, 1976, Berberian and King, 1981). Zagros Thrust Zone marks the boundary between the Zagros Fold Belt in the west and the Zagros Suture Zone in the east and is deeply rooted possibly to the Moho depth according to the geophysical and geological data (Agard et al, 2005, Azizi and Moinerazir, 2009). Along this zone magmatic activity and dismembered ophiolites occurred represented by Mawat group in the northeast Iraq comprising Mawat, Penjween, Bulfat and Pushtashan ophiolites with associated sediments, (Fig.1). These ophiolites were metamorphosed in the Late Cretaceous time and emplaced onto the Zagros Suture Zone during the Miocene time (Jassim and Goff, 2006). The study area is located within so-called Penjween ophiolite complex which comprises both mantle ultramafic sequence and cumulate gabbro

and volcanics of oceanic sequence (Al-Hassan and Habbard, 1985; Mohamed, 2007). The complex had suffered deformation and metamorphism that are associated with the igneous and sedimentary rocks. Amphibolite rocks appeared in the area as lenses and pods in contact with the overlying ultramafic rocks, mainly peridotite and serpentinized peridotite. However, no detail studies have been reported concerning these metamorphic rocks in the area.

The aim of the present study is to discuss the origin and thermo-barometric evolution of the amphibolite rocks utilizing mineralogy, mineral chemistry and geochemical data and to identify the protolith, tectonic setting of the emplacement and their relation to the associated igneous rocks in the area.

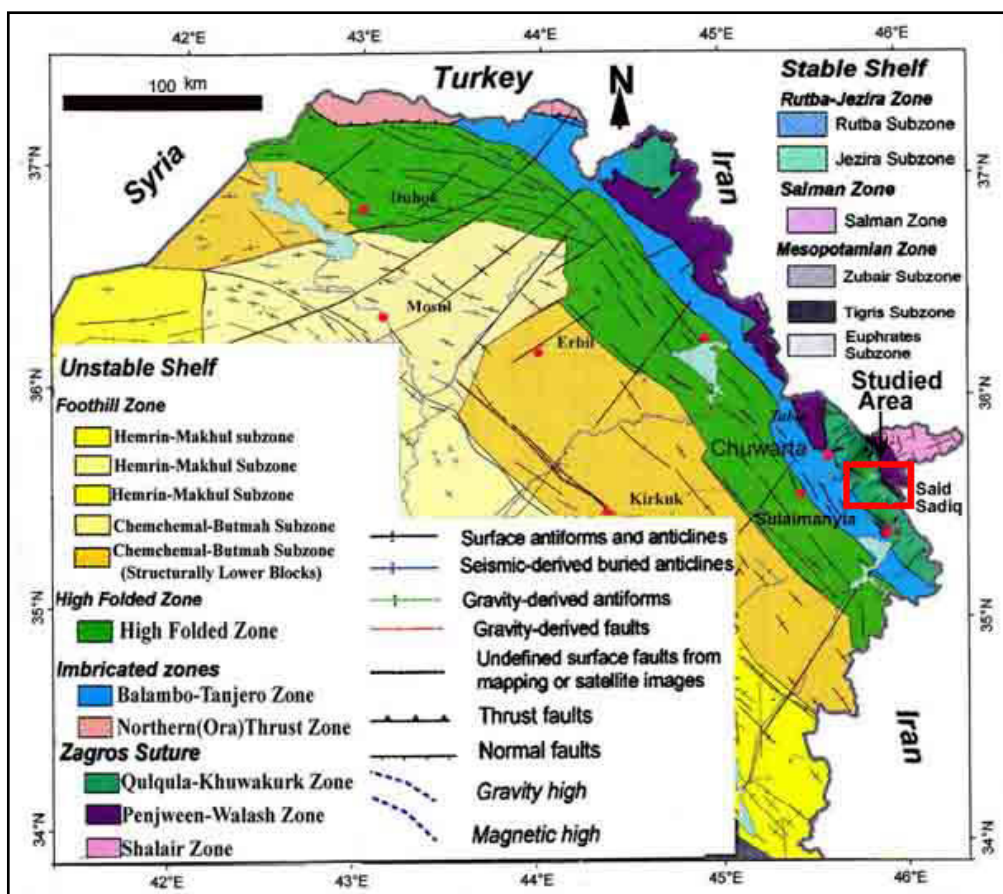


Figure -1: Generalized tectonic map of the Iraqi Zagros Thrust Zone showing the study area (Jassim and Goff, 2006).

2. Regional Geology

Zagros Orogenic Belt is considered a young continental belt that trends northwest-southeast. As a response to the collision between Eurasia and the advancing Arabian Plate during Mesozoic time, Zagros Mountain developed (Takin, 1972; Agard et al, 2005). According to Lippard et al (1986) continental breakup and the opening of the Neo-Tethys occurred during Traissic time while Stampfli et al (2001) suggested the Permian time for this opening phase. Northeast-dipping subduction of the Neo-Tethys oceanic lithosphere beneath the Sanandaj-Sirjan continental margin in Iran occurred during the Early Jurassic, (Dercourt et al, 1986) or Middle Jurassic (Agard et al (2005). Buday and Jassim(1987) and Jassim and Goff (2006) suggested Late Jurassic time for subduction event which is accompanied by the formation of volcanic arc close to the northern margin of the Arabian Plate. The intra-oceanic subduction continued until the collision with the northern Arabian Plate margin in the Late Cretaceous time accompanied by the emplacement of ophiolite onto the Arabian continental margin (Lippard et al,1986). After Late Cretaceous, the magmatic activity continued till Eocene time on the southern margin of the

Sanandaj-Sirjan block with the production of magmatic rocks. The continental collision caused the tectonic emplacement of these Eocene rocks onto the ophiolite sequences (Alavi, 1994; Allahyari et al 2010).

In northeast Iraq the Zagros Orogenic Belt is divided into the following northwest-southeast –trending domains: the Sanandaj-Sirjan, the Suture Zone, the Imbricated and the Fold-thrust Zone (Buday and Jassim, 1987). The Sanandaj-Sirjan zone represents the extreme northeastern part within the Iraqi-Iranian border but the major parts are in northwest Iran. It is a 150-200 km. wide and composed of deformed and metamorphosed Paleozoic-Mesozoic rocks which are intruded by Late Cretaceous to Paleocene plutons (Stockline, 1968; Alavi, 1994; Azizi and Jahaugiri, 2008). Shalair Zone is considered as an integral part of Sanadaj-Sirjan Zone in northeast Iraq and represents the innermost metamorphosed and volcanic units forming the structurally highest thrust sheets. The so-called Zagros Thrust Belt separates between the Zagros Suture Zone to the east and the Imbricated Zone to the west (Berberian and King, 1981; Jassim and Goff, 2006; Azizi and Moinevaziri, 2009). The Imbricated Zone consists of imbricated tectonic slices involving Qulqula radiolarite, Mawat igneous complexes, Penjween ophiolite complexes, Mesozoic and Cenozoic volcanic and sedimentary rocks as well as the thrust sheets from Sanandaj-Sirjan Zone. This zone represents a zone of thrust faults that have transported metamorphosed and non-metamorphosed Phanerozoic units of the Arabian continental margin as well as ophiolite complexes of the collisional suture zone from the northeast towards the interior parts of the Arabian Craton to the southwest (Aswad, 1999; Mohammed, 2007). Zagros Fold-Thrust Belt to the west represents the less strained part of the orogeny and consists of a pile of folded and faulted rocks of Paleozoic and Mesozoic successions which is overlain by Cenozoic siliciclastic and carbonate rocks that overlain metamorphosed Proterozoic Pan-African basement (Alavi, 2004; Mohammed, 2007).

Penjween area is located within so- called Penjween-Walash sub-zone within Zagros Suture Zone and it comprises volcano- sedimentary sequences formed during Cretaceous ocean spreading of the Neo-Tethys and is strongly affected by magmatism (Buday and Jassim, 1987). Paleocene arc volcanics and syn-tectonic basic intrusions formed during the final closure of Neo-Tethys Ocean during Paleocene-Eocene time (Aswad, 1999). The zone is thus represents the remnant of the Neo-Tethys which was thrust over the Arabian Plate during Miocene –Pliocene. The Penjween-Walash sub-zone forms an almost continuous belt along the Iraqi-Iranian border and consists of three thrust sheets: the structurally lowest Napurdan, the middle Walash and the upper Qandil. The upper Qandil thrust sheet comprises basic igneous massifs including Penjween, Mawat, Bulfat and Pushtashan. The study area is located within this zone.

Penjween igneous complex is situated to the southwest of Penjween town about 40 km. to the east of Sulaimaniye city, Kurdistan region between latitudes ($35^{\circ} 36' 16.4''$ - $35^{\circ} 37' 15.6''$ N) and longitudes ($45^{\circ} 54' 40.4''$ - $45^{\circ} 55' 54''$ E), (Fig.2). It has a very complicated topography consisting of rugged mountains with elevation reaching about 1484 m. in the root peak with very steep valleys. 15-16 pods of amphibolite rocks were observed and sampled in the area. They occur as discontinuous bodies of different sizes and shapes in contact with peridotite and serpentized peridotite (Fig.3). These amphibolite pods are of lensoid shape with variable dimensions generally ranging from 2-3 m. long and 0.5-2 m. thick of dark olive green color. They have sharp contacts with the ultramafics and some have large scale lamination due to the gradation in grain size (Fig.4) with some cut by 2mm. chlorite veins (Fig.5) and one in contact with albitite dyke. In addition, one amphibole gabbro dyke of 1m. thick is recognized. This dyke is vertically trending and cut by serpentinite which grades into pure amphibolite (Fig.6).

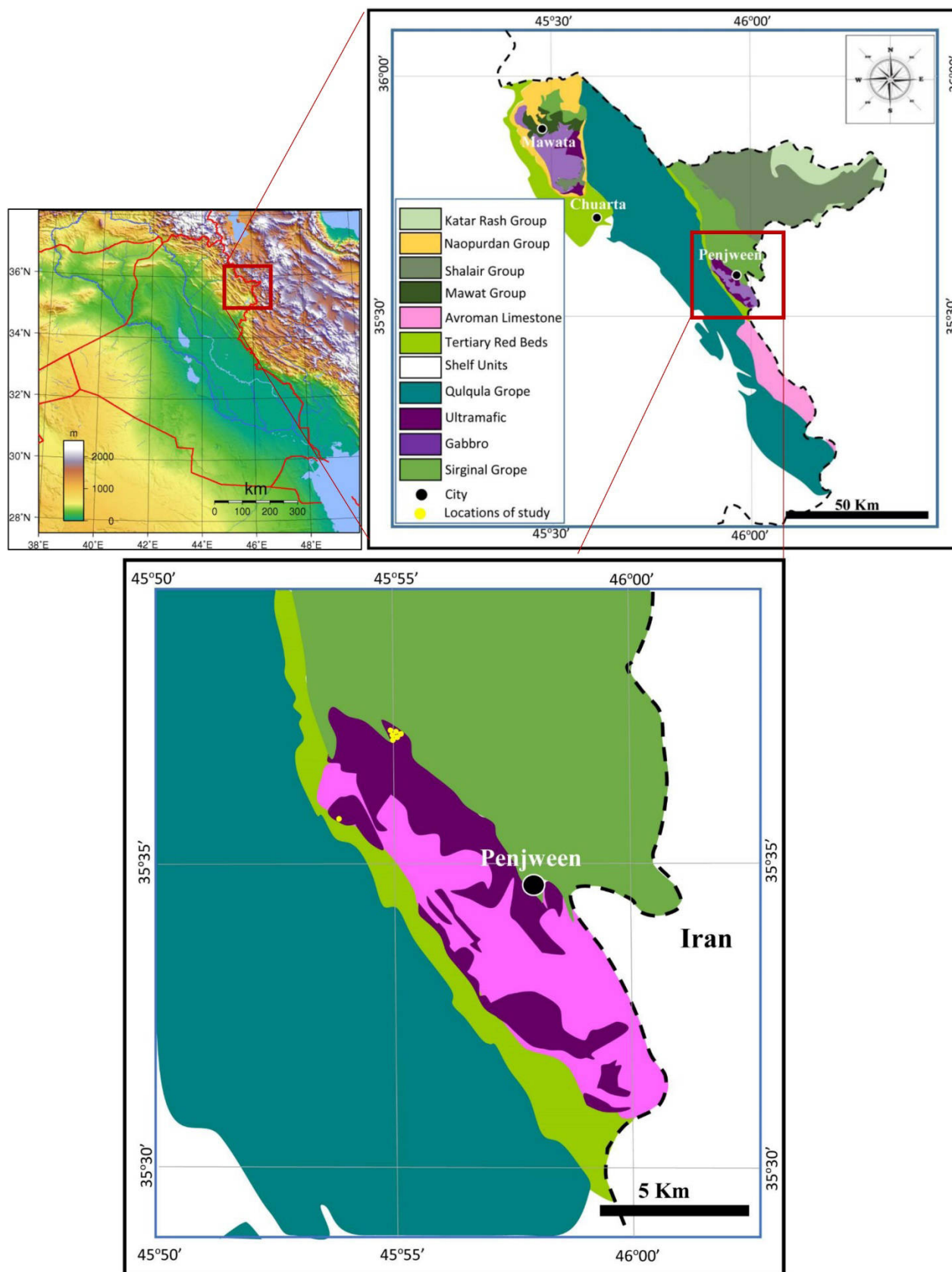


Figure-2: Geologic map of Penjween showing samples locations.



Figure-3: Field distribution of the amphibolite outcrops.



Figure-4: Large scale grain size lamination within one of the amphibolite outcrop.

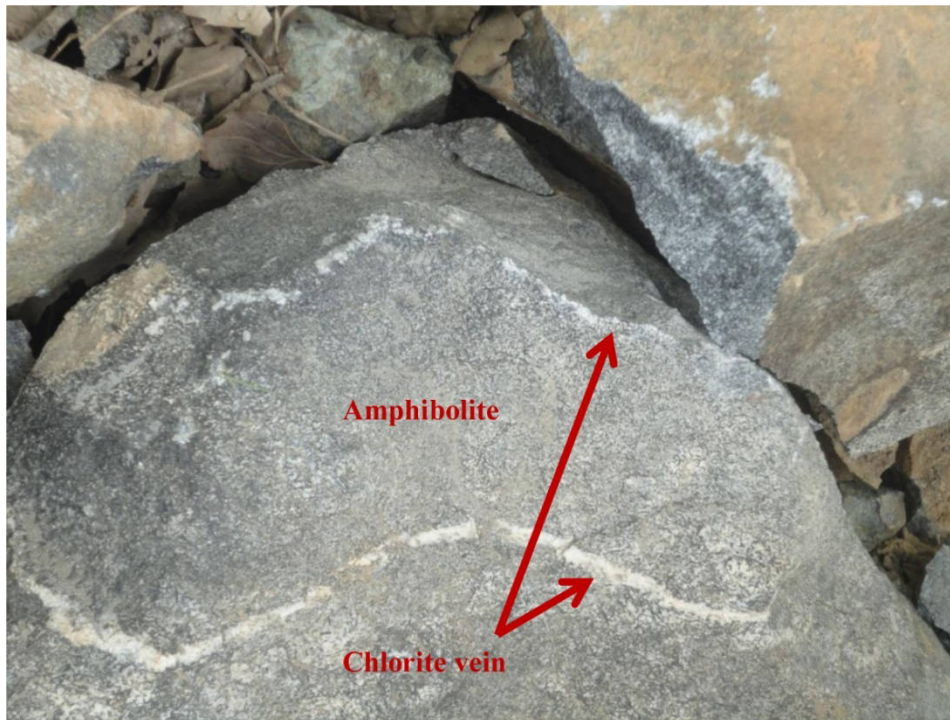


Figure-5: Chlorite veins cutting one of the amphibolite outcrop.

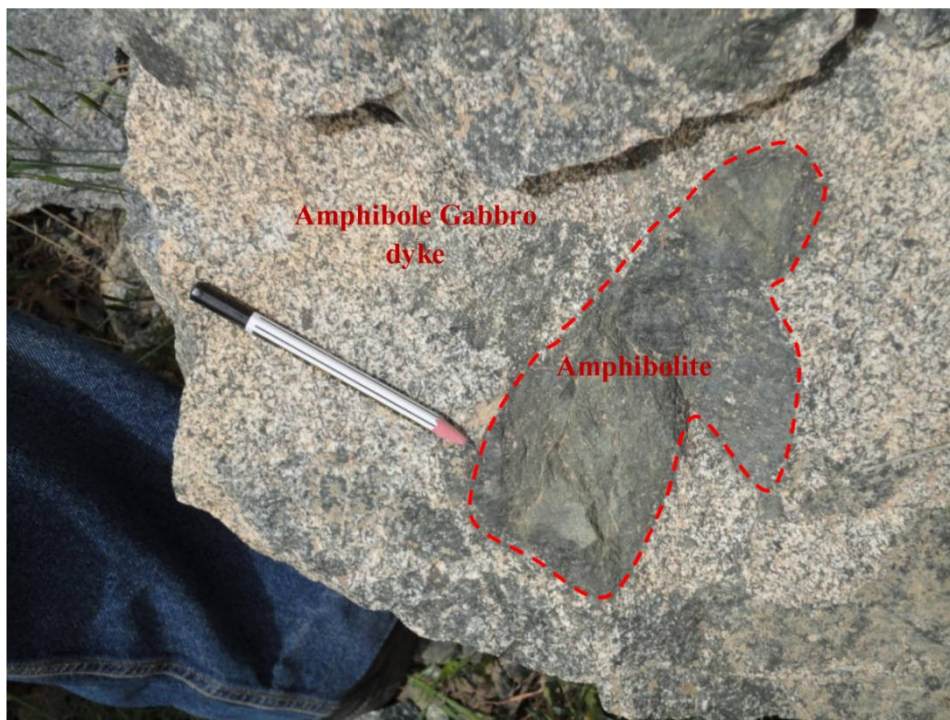


Figure-6: Amphibole gabbro dyke.

3. Analytical Methods

Twenty samples of amphibolites and serpentized peridotites among them 14 samples for amphibolite rocks are collected with one amphibole gabbro dyke sample and one albitite dyke sample. Mineral chemical analyses were carried out using wavelength dispersive microprobe (JEOL Super probe JXA- 8800) at the Cooperation Research Center, Kanazawa University, Japan. Raw data for each element were corrected using ZAF program. Analytical conditions are: 15 KV for acceleration voltage, 20n°A for beam current and 3 µm. for beam diameter. The counting time is 20 sec. on the peak of the characteristic X-ray for each element. Analytical errors are <0.1 wt. % for major and minor elements respectively. The results of the chemical analyses for amphiboles and plagioclases are listed in table-1 and 2. For whole rock chemical analyses,(table-3) the major elements are determined by ICP-MS (ME-ICP-06), the trace and REE are determined by ICP-MS (ME-MS 81) at ALS Lab Group in Seville-Spain. For major elements 0.3 gm. powder sample for each is fused with LiBO₂ and then dissolved in 5% HNO₃. For trace and rare earth elements (REE), rock powder for each sample was dissolved in 4% acid digestion. Analytical errors for the major oxides range from 0.001-0.01 % and for trace elements range from 1.1-0.5 and 0.01-0.5 for REE.

4. Petrography and Mineral Chemistry

4.1 Amphibolite

Amphibole and plagioclase are the major constituents of these amphibolites with amphibole comprising 55-60 % and plagioclase 30-35 % (by volume). Both primary and secondary amphiboles are observed. The primary amphiboles are mostly euhedral to subhedral-shaped having well developed cleavage with few inclusions of iron oxides and lack sub-grain development along the larger grains (Fig.-7a). On the other hand, the secondary amphiboles are anhedral- shaped of variable sizes with oxidation along the cleavage traces and grains boundary, with relicts of the original pyroxenes and amphiboles (Fig.-7-b-,c). According to Leaks et al (1997), the amphiboles are calcic and range in composition between Mg- hornblende and tschermakite (Fig.9) with Mg* ranging between 0.62-0.76.

Plagioclase modally constitutes average 35%, of variable sizes, idiomorphic to sub-idiomorphic, some have inclusions and some are fresh and some are partly sericitized (Fig.-7d). The larger grains show polysynthetic twinning, in contrast, the smaller grains lack twinning. The composition of the plagioclase is Na-rich ranging between oligoclase (An_{23.9} Ab_{75.9} Or_{0.2}) and (An_{1.7} Ab_{97.9} Or_{0.4}), (Fig.10 and table 3).

Clinopyroxene modally forms 7.5%, generally fine subhedral to anhedral partly altered to secondary amphibole and chlorite (Fig.-7-e-f). Quartz makes 3% by volume, mostly fine and some show undulose extinction, together with fine zircon, apatite, titanite, ilmenite and opaques form the accessory mineral phases (Fig.-7g). The presence of titanite and ilmenite in these amphibolites indicates high temperature condition of metamorphism (Raase et al, 1986; Ernst and Liu, 1998) hence, the appearance of Ti- bearing phases is considered as temperature indicator. Opaques including Fe-Ti-oxides of primary euhedral and secondary fine disseminated that associate with altered pyroxenes and amphiboles are observed, and there is generally a strong association between oxide-rich regions and highly deformed and altered regions (Fig.-7-h,i).

The amphibolites are characterized by different textural relationships with rare relict textures of their protolith as porphyroblastic with amphibole and plagioclase as the main phenocrysts but also appear as fine laths together with the accessory phases in the groundmass. In addition, granoblastic, blasto-ophitic, granonemato-blastic and poikilo-blastic textures also observed. Fine epidote, quartz, and calcite inclusions appeared enclosed within the poikilo-blastic amphiboles. The presence of fine actinolite crystals around the porphyroblastic and poikiloblastic amphiboles as well as chlorite and sericite after amphiboles and plagioclase respectively indicates some sort of retrogressive metamorphism.

According to the petrographic study, these amphibolites are grouped into two assemblages:

- | | |
|---|----|
| Hornblende+ plagioclase+ clinopyroxene+ quartz+ titanite± zircon± apatite+ iron oxides. | -1 |
| Hornblende+ plagioclase+ quartz+ titanite± apatite ± zircon + iron oxides. | -2 |

The second assemblage is the most widespread within the majority of study sample and show more intense alteration.

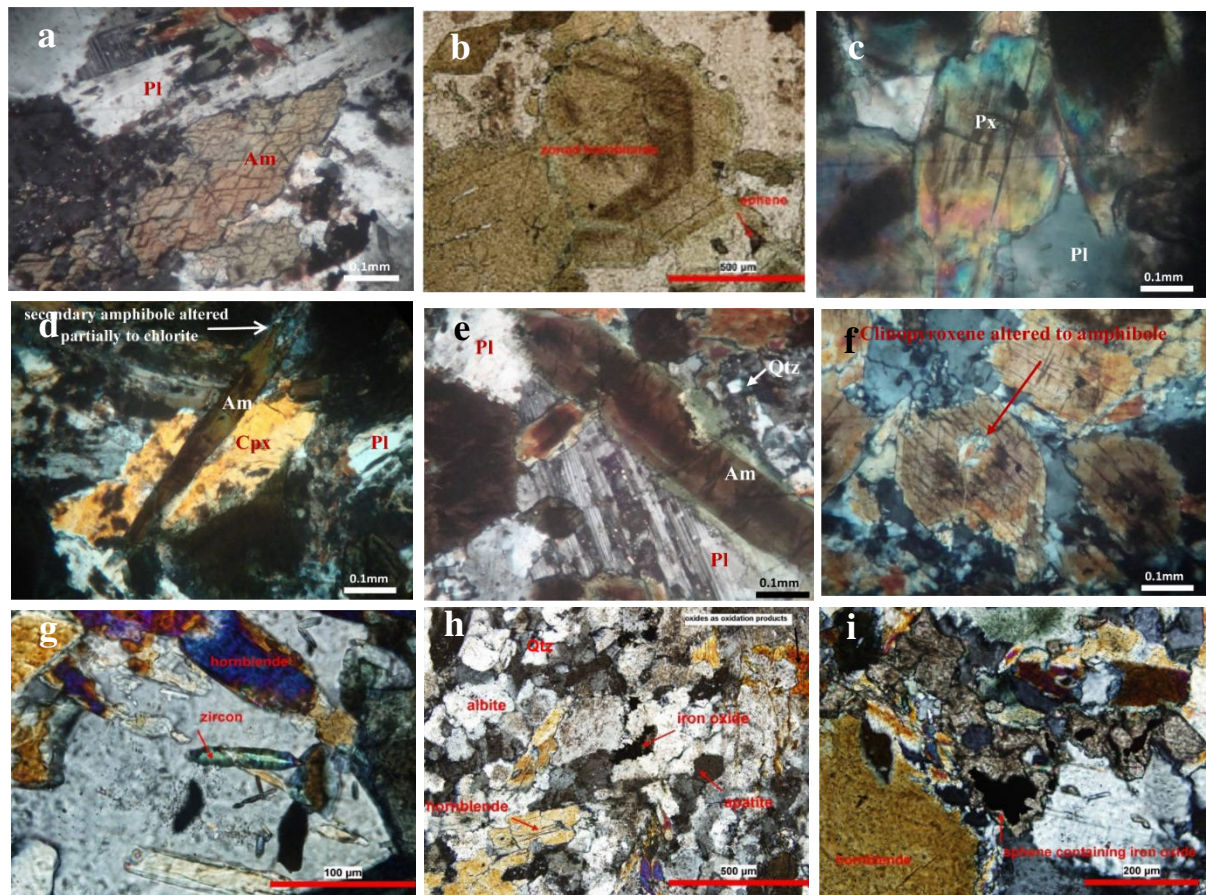


Figure-7-a-i: Photomicrographs of the amphibolite rocks:

- a-** Primary amphibole and plagioclase forming granoblastic texture. XPL. Sample PA11.
- b-** Secondary amphibole penetrating primary clinopyroxene. XPL. Sample PA12.
- c-** Zoned amphibole crystal with subgrains around it. XPL. Sample PA2.
- d-** Plagioclase and amphibole phenocrysts in groundmass of the same minerals with quartz. Some of the quartz show undulose extinction. XPL. Sample PA2.
- e-** Granoblastic texture of clinopyroxene and plagioclase with secondary amphiboles. XPL. Sample PA1.
- f-** Relict of clinopyroxene surrounded by secondary amphibole. XPL. Sample PA1.
- g-** Poikiloblastic texture, zircon inclusions with sericite patches within large plagioclase grain. XPL. Sample PA12.
- h-** Granoblastic texture showing distribution of the major and accessory mineral phases. XPL. Sample PA10.
- i-** Porphyroblastic texture with large amphibole and plagioclase phenocrysts. Also shows the association of titanite (sphene) with iron oxides. XPL. Sample PA14.

4-2. Amphibole- gabbro dyke

Hornblende (57.7%) and clinopyroxene are the major mafic phases, (Fig.8-a- b). The clinopyroxene is partially altered into amphibole and appeared as relict within amphibole. Prismatic euhedral- subhedral hornblende observed with some showing secondary twinning (Fig.8-c). Plagioclase modally form (30- 35%) mostly fresh of andesine composition with few showing partial alteration to epidote and sericite. Fine euhedral apatite, titanite (sphene) and iron oxides are the common accessory minerals (Fig.8-d). Ophitic, subophitic and intergranular textures are common.

Table-1: Continued

| Element | A2.9 | A2.10 | A3.1 | A3.2 | A3.3 | A3.4 | A3.5 | A3.6 | A3.7 | A3.8 | A3.9 | A3.10 | A3.11 | A3.12 | A3.13 | A3.14 |
|---------------------------|-------|-------|--------------|--------------|--------------|-------|--------------|--------------|--------------|--------------|-------|-------|-------|-------|-------|-------|
| SiO2 | 45.81 | 46.23 | 43.82 | 44.57 | 38.83 | 40.95 | 39.01 | 40.32 | 40.19 | 47.48 | 44.69 | 46.07 | 43.36 | 45.86 | 45.29 | 43.09 |
| TiO2 | 0.95 | 2.78 | 0.84 | 0.78 | 2.36 | 0.84 | 0.92 | 0.91 | 0.92 | 0.48 | 0.76 | 0.55 | 0.84 | 0.55 | 0.62 | 0.85 |
| AL2O3 | 10.22 | 8.40 | 12.16 | 11.76 | 15.49 | 16.02 | 15.40 | 15.36 | 14.98 | 8.88 | 11.60 | 10.55 | 12.15 | 10.34 | 10.95 | 12.59 |
| FeO | 9.80 | 8.55 | 10.02 | 9.80 | 12.49 | 10.98 | 10.88 | 11.01 | 10.93 | 9.10 | 9.87 | 9.34 | 9.75 | 9.70 | 9.00 | 10.30 |
| MnO | 0.17 | 0.18 | 0.15 | 0.17 | 0.18 | 0.17 | 0.16 | 0.17 | 0.15 | 0.19 | 0.18 | 0.17 | 0.16 | 0.21 | 0.14 | 0.15 |
| MgO | 15.15 | 15.61 | 15.15 | 15.43 | 12.15 | 13.39 | 12.82 | 13.63 | 13.41 | 16.38 | 15.45 | 15.86 | 15.14 | 15.59 | 15.89 | 14.68 |
| CaO | 12.71 | 13.23 | 13.47 | 13.46 | 13.58 | 13.41 | 13.35 | 13.38 | 13.54 | 13.49 | 13.36 | 12.39 | 13.33 | 12.26 | 12.29 | 13.57 |
| Na2O | 1.76 | 1.38 | 1.48 | 1.50 | 1.49 | 2.10 | 1.97 | 2.09 | 1.90 | 0.74 | 1.39 | 0.97 | 1.69 | 2.29 | 2.16 | 1.73 |
| K2O | 0.41 | 0.20 | 0.17 | 0.14 | 0.75 | 0.26 | 0.27 | 0.28 | 0.25 | 0.15 | 0.14 | 0.15 | 0.16 | 0.20 | 0.17 | 0.19 |
| Total | 97.02 | 96.63 | 97.42 | 97.72 | 97.34 | 98.36 | 95.01 | 97.23 | 96.38 | 97.20 | 97.58 | 97.50 | 97.07 | 97.20 | 96.62 | 97.53 |
| Cr2O3 | 0.01 | 0.03 | 0.11 | | 0.06 | 0.19 | 0.19 | 0.05 | 0.06 | 0.28 | 0.10 | 0.14 | 0.44 | 0.16 | 0.07 | 0.08 |
| Si | 6.00 | 6.12 | 5.91 | 6.12 | 6.69 | 6.75 | 6.87 | 6.50 | 6.67 | 6.37 | 6.68 | 6.61 | 6.31 | 6.61 | 6.98 | 6.57 |
| [Al] ⁺⁴ | 2.00 | 1.88 | 2.09 | 1.88 | 1.31 | 1.25 | 1.13 | 1.5 | 1.33 | 1.63 | 1.32 | 1.39 | 1.69 | 1.39 | 1.02 | 1.43 |
| [Al] ⁺⁶ | 0.42 | 0.38 | 0.55 | 0.45 | 0.45 | 0.19 | 0.38 | 0.49 | 0.47 | 0.47 | 0.46 | 0.49 | 0.53 | 0.45 | 0.34 | 0.55 |
| Fe | 1.61 | 1.57 | 1.68 | 1.55 | 1.20 | 1.04 | 1.10 | 1.20 | 1.13 | 1.20 | 1.18 | 1.10 | 1.26 | 1.28 | 1.14 | 1.31 |
| Ti | 0.27 | 0.30 | 0.20 | 0.22 | 0.10 | 0.31 | 0.05 | 0.08 | 0.06 | 0.09 | 0.06 | 0.07 | 0.09 | 0.05 | 0.03 | 0.06 |
| Mn | 0.03 | 0.02 | 0.03 | 0.05 | 0.02 | 0.02 | 0.02 | 0.02 | 0.02 | 0.02 | 0.03 | 0.02 | 0.02 | 0.02 | 0.02 | 0.02 |
| Mg | 2.75 | 2.81 | 2.69 | 2.80 | 3.30 | 3.39 | 3.53 | 3.35 | 3.42 | 3.31 | 3.38 | 3.46 | 3.20 | 3.27 | 3.48 | 3.14 |
| Ca | 1.87 | 1.78 | 1.85 | 1.85 | 1.83 | 1.91 | 1.78 | 1.77 | 1.77 | 1.78 | 1.76 | 1.77 | 1.82 | 1.88 | 1.93 | 1.83 |
| Na | 0.42 | 0.36 | 0.48 | 0.46 | 0.38 | 0.67 | 0.37 | 0.76 | 0.70 | 0.51 | 0.43 | 0.39 | 0.66 | 0.84 | 0.60 | 0.47 |
| K | 0.21 | 0.19 | 0.17 | 0.14 | 0.08 | 0.04 | 0.03 | 0.03 | 0.03 | 0.03 | 0.04 | 0.03 | 0.04 | 0.04 | 0.03 | 0.04 |
| Mg/(Mg+Fe ⁺²) | 0.63 | 0.64 | 0.62 | 0.64 | 0.73 | 0.76 | 0.76 | 0.74 | 0.75 | 0.73 | 0.74 | 0.76 | 0.72 | 0.72 | 0.75 | 0.71 |
| Type | Mg-Hb | Mg-Hb | Tschermakite | Tschermakite | Tschermakite | | Tschermakite | Tschermakite | Tschermakite | Tschermakite | Mg-Hb | Mg-Hb | Mg-Hb | Mg-Hb | Mg-Hb | Mg-Hb |

Table-2: Chemical analyses of plagioclase

| Element | P1.1 | P1.2 | P1.3 | P1.4 | P2.1 | P2.2 | P2.3 | P2.4 |
|---------|------------|------------|------------|------------|--------|--------|--------|--------|
| SiO2 | 60.52 | 61.33 | 57.40 | 61.02 | 66.90 | 66.31 | 66.36 | 65.30 |
| TiO2 | 0.02 | 0.00 | 0.03 | 0.00 | 0.05 | 0.00 | 0.03 | 0.04 |
| AL2O3 | 24.82 | 24.14 | 21.84 | 24.16 | 20.87 | 20.357 | 21.02 | 20.4 |
| Cr2O3 | 0.01 | 0.00 | 0.03 | 0.00 | 0.02 | - | - | - |
| FeO | 0.03 | 0.18 | 0.06 | 0.13 | 0.25 | 0.19 | 0.15 | 0.17 |
| MnO | 0.00 | 0.00 | 0.01 | 0.01 | 0.01 | 0.01 | - | 0.01 |
| MgO | 0.01 | 0.00 | 0.00 | 0.00 | 0.01 | 0.01 | 0.01 | 0.02 |
| CaO | 5.68 | 4.60 | 4.18 | 4.21 | 0.22 | 0.42 | 0.58 | 0.38 |
| Na2O | 9.28 | 10.33 | 9.22 | 10.65 | 13.17 | 12.43 | 12.33 | 12.98 |
| K2O | 0.04 | 0.05 | 0.06 | 0.05 | 0.07 | 0.18 | 0.08 | 0.07 |
| NiO2 | 0.01 | 0.00 | 0.00 | 0.00 | 0.01 | - | - | - |
| Total | 100.42 | 100.63 | 92.82 | 100.24 | 100.74 | 100.41 | 99.87 | 99.96 |
| Si | 2.69 | 2.72 | 2.75 | 2.72 | 2.93 | 2.91 | 0.02 | 2.89 |
| Ti | 0.00 | - | 0.00 | 0.00 | 0.00 | 0.00 | - | - |
| Al | 1.30 | 1.26 | 1.23 | 1.27 | 1.03 | 1.08 | 1.31 | 1.10 |
| Cr | 0.00 | - | 0.00 | - | 0.00 | - | - | - |
| Fe | 0.00 | 0.01 | 0.00 | 0.01 | 0.01 | 0.01 | 0.00 | 0.01 |
| Mn | - | - | 0.00 | - | 0.00 | 0.00 | 0.00 | 0.00 |
| Mg | 0.00 | - | - | 0.00 | 0.00 | 0.00 | 0.00 | 0.00 |
| Ca | 0.27 | 0.22 | 0.21 | 0.20 | 0.01 | 0.02 | 0.00 | 0.02 |
| Na | 0.80 | 0.89 | 0.86 | 0.92 | 1.12 | 1.06 | 0.01 | 1.11 |
| K | 0.00 | 0.00 | 0.00 | 0.00 | 0.00 | 0.01 | 0.00 | 0.00 |
| Ni | 0.00 | - | - | 0.00 | 0.00 | - | - | - |
| Total | 5.06 | 5.10 | 5.06 | 5.11 | 5.11 | 5.08 | 5.33 | 5.12 |
| Type | Oligoclase | Oligoclase | Oligoclase | Oligoclase | Albite | Albite | Albite | Albite |

Mineral chemistry

An₂₄
Ab₇₄
Or_{0.2}

An₂₀
Ab₈₀
Or_{0.2}

An₂₀
Ab₈₀
Or_{0.3}

An₁₈
Ab₈₂
Or_{0.2}

An₁
Ab₉₈
Or_{0.3}

An₂
Ab₉₇
Or₁

An₆
Ab₉₇
Or_{0.4}

An₂
Ab₉₈
Or_{0.4}

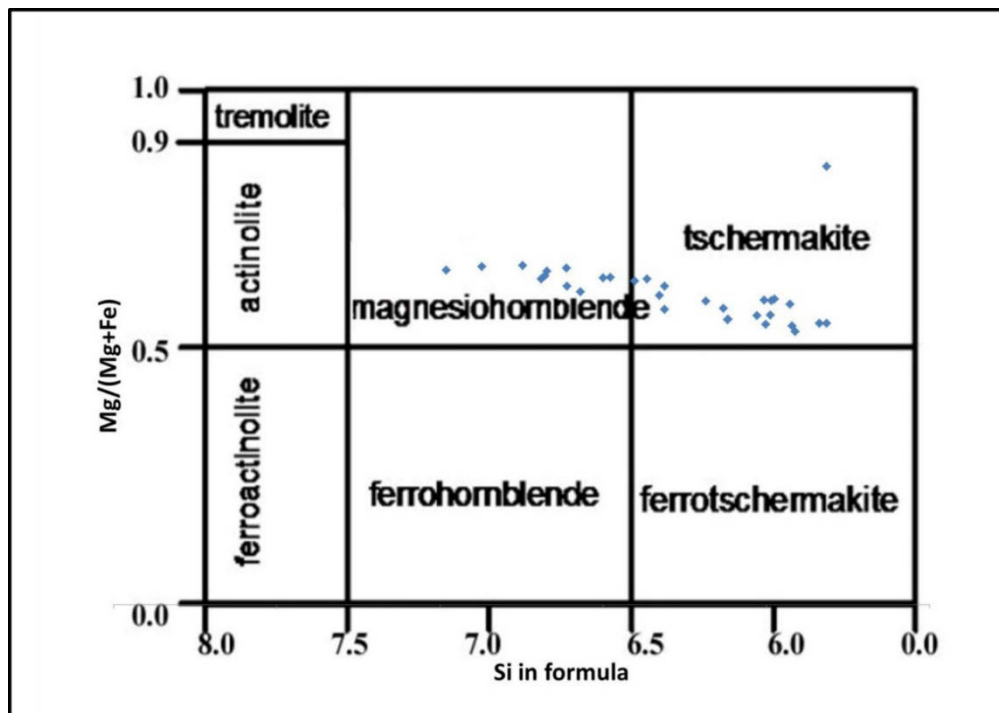


Figure 9: Chemical classification of amphiboles, (after Leak *et al* ,1997). Apuf= atom per unit formula.

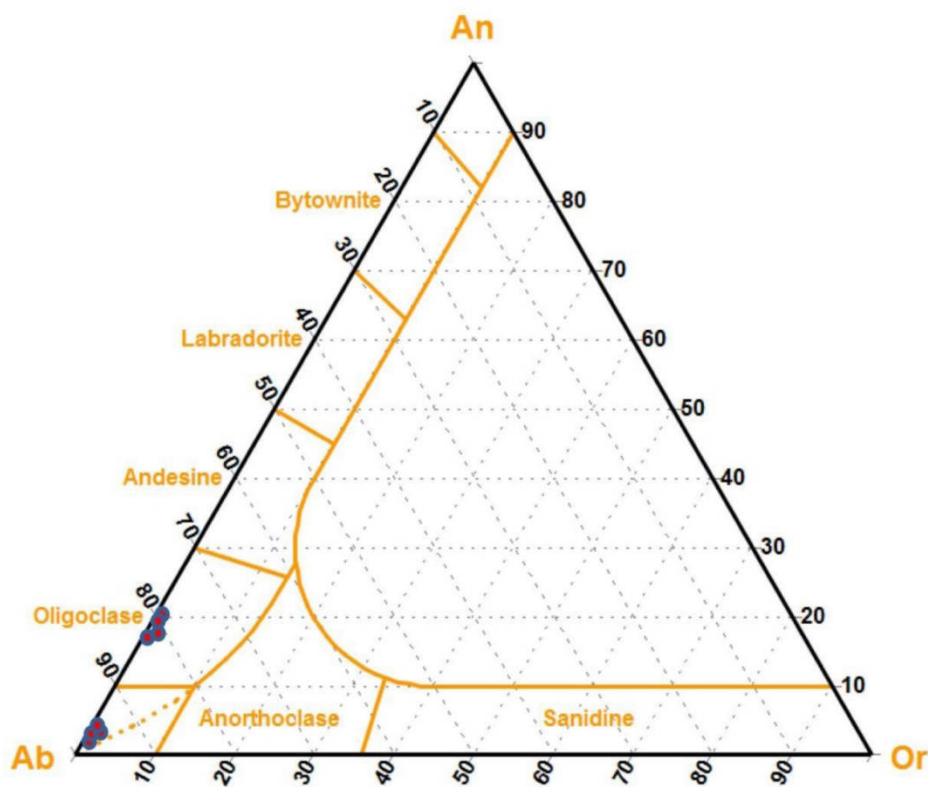


Figure 10: Chemical classification of plagioclase,(after Deer *et al* 1963). Ab=albite, An=anorthite, Or=orthoclase.

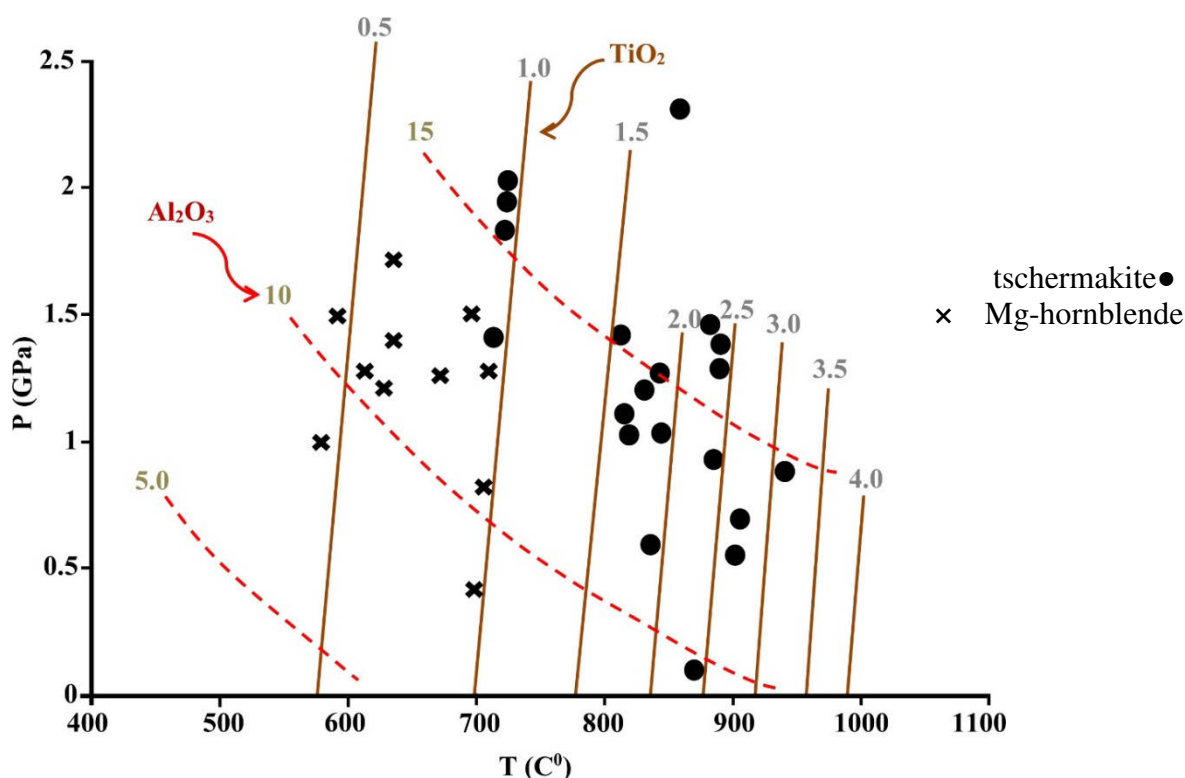


Figure 11: Al_2O_3 and TiO_2 isopleths (in wt%) of analyzed amphiboles on P-T diagram (after Ernst and Liu, 1998).

5. Whole rock geochemistry

Bulk chemical analyses were performed for fourteen representative amphibolite samples based on the selection of the least altered (table-3). The geochemical features of these amphibolites are described by using those elements which are virtually immobile during alteration and metamorphism. These amphibolites are characterized by: SiO_2 (42.5-58.7%), Al_2O_3 (12.95-16.65%), FeO (4.5-12.9%), CaO (4.97-13.4%), MgO (5.23-14.25%), and TiO_2 (0.47-1.44%), with exception of two samples (PA4 and PA14) which have very low SiO_2 , Al_2O_3 and MgO. The amphibolites exhibit distinct more or less coherent positive and negative correlations of the major oxides and trace elements with SiO_2 and MgO (table-3, Figs. 12a-h) reflecting amphibole, plagioclase, clinopyroxene and Fe-Ti-oxide crystallization. In general, the geochemical criteria and relationships of these amphibolites confirm their igneous origin; the relationship between TiO_2 -Cr proposed by Leak (1964) shows an igneous protolith (ortho) by the plot of all samples outside the sedimentary protolith (para), (Fig.13-a). Furthermore, the high $\text{Cr/Th} \geq 100$; the low $\text{Th/La} \sim 0.05$, and $\text{Zr/TiO}_2 \sim 0.013$; the high Ni (ava.173.3 ppm) and Cr (ava.397.5ppm), (table-3) are all characteristics of typical igneous protolith (Taylor and Mc Lennan, 1985; Rollinson, 1996). Accordingly, on SiO_2 - K_2O diagram of Peccerillo and Taylor (1976), the data fall within low-K tholeiite field (Fig.13-b) and on Zr-Y diagram of Barret and Maclean (1999) within tholeiitic basalt field with an average $\text{Zr/Y} = 2.9$ except three samples which fall within the transitional field (Fig.13-c). These characteristics of the amphibolites indicate their formation through pyroxene and plagioclase fractionations with original protolith composition that correspond to sub-alkali basalt and andesite on Nb/Y-Zr/ TiO_2 diagram (Fig.13-d) proposed by Wichester and Floyd (1977).

Table-3: Whole rock chemical analyses of Penjween amphibolites

| SAMPLE | SiO ₂ | Al ₂ O ₃ | Fe ₂ O ₃ | CaO | MgO | Na ₂ O | K ₂ O | Cr ₂ O ₃ | TiO ₂ | MnO | P ₂ O ₅ | SrO | BaO | LOI | Total |
|--------|------------------|--------------------------------|--------------------------------|------|-------|-------------------|------------------|--------------------------------|------------------|------|-------------------------------|-------|-------|------|-------|
| Number | % | % | % | % | % | % | % | % | % | % | % | % | % | % | % |
| P.A1 | 47.6 | 15.65 | 11.95 | 9.41 | 7.79 | 4.81 | 0.31 | 0.04 | 1.24 | 0.16 | 0.16 | 0.06 | 0.01 | 1.49 | 100.5 |
| P.A2 | 48.2 | 15.05 | 11.8 | 9.21 | 8.54 | 4.64 | 0.27 | 0.05 | 1.13 | 0.16 | 0.21 | 0.08 | 0.01 | 1.8 | 101 |
| P.A4 | 34.6 | 0.26 | 8.15 | 0.11 | 40.5 | <0.01 | <0.01 | 0.64 | 0.01 | 0.1 | 0.02 | <0.01 | <0.01 | 15.7 | 100 |
| P.A5 | 42.5 | 12.95 | 12.9 | 11.9 | 13.55 | 2.95 | 0.24 | 0.09 | 1.17 | 0.18 | 0.37 | 0.02 | <0.01 | 1.89 | 100.5 |
| P.A8 | 45.1 | 16.65 | 9.52 | 13.4 | 8.65 | 3.64 | 0.26 | 0.04 | 0.96 | 0.14 | 0.2 | 0.11 | 0.04 | 2.78 | 101.5 |
| P.A9 | 48.9 | 14.45 | 11 | 9.32 | 8.73 | 4.59 | 0.36 | 0.07 | 1.12 | 0.17 | 0.18 | 0.06 | 0.01 | 1.7 | 100.5 |
| P.A10 | 48.1 | 15.3 | 10.55 | 8.7 | 7.22 | 5.06 | 0.21 | 0.04 | 1.16 | 0.14 | 0.16 | 0.1 | 0.01 | 1.58 | 98.3 |
| P.A11 | 46.2 | 13.05 | 11.8 | 9.39 | 10.05 | 4.03 | 0.22 | 0.08 | 1.01 | 0.18 | 0.15 | 0.05 | 0.01 | 1.79 | 98 |
| P.A12 | 47.4 | 13.35 | 10.05 | 10.7 | 9.92 | 3.91 | 0.33 | 0.06 | 1.44 | 0.14 | 0.33 | 0.11 | 0.01 | 1.09 | 98.8 |
| P.A14 | 40.7 | 0.94 | 7.86 | 0.9 | 38.7 | 0.23 | 0.01 | 0.37 | 0.03 | 0.1 | <0.01 | <0.01 | <0.01 | 8 | 97.8 |
| P.A15 | 55.7 | 15.7 | 6.81 | 6.85 | 5.9 | 6.94 | 0.22 | 0.02 | 0.64 | 0.1 | 0.07 | 0.1 | 0.03 | 1.19 | 100.5 |
| P.A16 | 58.3 | 14.35 | 4.6 | 6.51 | 7.76 | 6.97 | 0.08 | 0.04 | 0.66 | 0.08 | 0.2 | 0.17 | 0.03 | 1.2 | 101 |
| P.A17 | 58.7 | 16.35 | 4.53 | 4.97 | 5.23 | 7.91 | 0.09 | 0.03 | 0.47 | 0.06 | 0.12 | 0.18 | 0.01 | 0.8 | 99.5 |
| P.A20 | 42.8 | 13.5 | 11.45 | 11.9 | 14.25 | 3.42 | 0.17 | 0.13 | 1.32 | 0.16 | 0.29 | 0.02 | <0.01 | 1 | 100.5 |

| SAMPLE | Ag | Ba | Ce | Co | Cr | Cs | Cu | Dy | Er | Eu | Ga | Gd | Hf | Ho | La | Lu | Mo | Nb | Nd | Ni |
|--------|-----|-------|------|-------|------|-------|-----|-------|-------|-------|------|------|------|-------|------|------|-----|------|------|------|
| Number | ppm | ppm | ppm | ppm | ppm | ppm | ppm | ppm | ppm | ppm | ppm | ppm | ppm | ppm | ppm | ppm | ppm | ppm | ppm | ppm |
| P.A1 | <1 | 74.8 | 27.4 | 46 | 290 | 0.52 | 66 | 4.03 | 2.2 | 1.34 | 19.6 | 4.07 | 2.4 | 0.83 | 12.8 | 0.31 | <2 | 7.4 | 16.7 | 152 |
| P.A2 | <1 | 62.7 | 27.3 | 53.6 | 380 | 0.58 | 79 | 3.73 | 2.09 | 1.26 | 18.3 | 3.76 | 2.2 | 0.76 | 12.8 | 0.29 | <2 | 7 | 16.4 | 193 |
| P.A4 | <1 | 1.3 | <0.5 | 124.5 | 4560 | <0.01 | <5 | <0.05 | <0.03 | <0.03 | 0.7 | 0.05 | <0.2 | <0.01 | <0.5 | 0.01 | <2 | <0.2 | 0.1 | 1975 |
| P.A5 | <1 | 29.1 | 32 | 61.7 | 620 | 0.1 | 20 | 4.26 | 2.34 | 1.61 | 17 | 4.07 | 2.6 | 0.84 | 15.6 | 0.29 | <2 | 8.4 | 17.1 | 263 |
| P.A8 | <1 | 329 | 51.1 | 35.8 | 270 | 0.25 | 31 | 4.37 | 2.36 | 2.51 | 16.4 | 4.44 | 3.5 | 0.86 | 25.7 | 0.34 | <2 | 12.2 | 25.3 | 140 |
| P.A9 | <1 | 100.5 | 28 | 50.8 | 470 | 0.72 | 79 | 3.57 | 2.1 | 1.31 | 20.4 | 3.92 | 2.7 | 0.73 | 13.5 | 0.29 | <2 | 6.4 | 14.6 | 189 |
| P.A10 | <1 | 63.6 | 29.6 | 49.8 | 290 | 0.96 | 135 | 4.06 | 2.3 | 1.41 | 18.8 | 4.25 | 2.6 | 0.81 | 14.4 | 0.31 | <2 | 6.7 | 14.7 | 116 |
| P.A11 | <1 | 54.9 | 24 | 48.2 | 550 | 0.08 | 53 | 3.72 | 2.07 | 1.28 | 19.3 | 3.89 | 2.2 | 0.72 | 11.3 | 0.28 | <2 | 4.9 | 12.7 | 235 |
| P.A12 | <1 | 91.3 | 52 | 49.5 | 410 | 0.57 | 66 | 4.14 | 2.15 | 1.89 | 17.1 | 5.44 | 3.6 | 0.79 | 24.9 | 0.26 | 2 | 12.2 | 26.4 | 154 |
| P.A14 | <1 | 5.2 | 1.4 | 109 | 2410 | 0.14 | <5 | 0.06 | 0.03 | 0.03 | 1.1 | 0.06 | 0.3 | 0.01 | 0.9 | 0.01 | <2 | 0.2 | 0.6 | 1865 |
| P.A15 | <1 | 283 | 16.3 | 23.7 | 130 | 2.19 | 14 | 2.91 | 1.65 | 1.14 | 15.7 | 3.06 | 2.7 | 0.62 | 7.4 | 0.21 | <2 | 1.9 | 10.7 | 36 |
| P.A16 | <1 | 288 | 44.1 | 20.9 | 260 | 0.28 | 13 | 1.66 | 0.76 | 1.05 | 17.8 | 2.7 | 3.9 | 0.31 | 21.2 | 0.1 | 2 | 3.7 | 22.8 | 204 |
| P.A17 | <1 | 115.5 | 20.8 | 19.6 | 200 | 0.51 | <5 | 1.51 | 0.88 | 0.61 | 17.7 | 1.71 | 2.7 | 0.33 | 10.6 | 0.12 | <2 | 1.5 | 10.3 | 59 |
| P.A20 | <1 | 34.6 | 94.9 | 59.4 | 900 | 0.08 | 75 | 5.36 | 2.96 | 2.51 | 16.6 | 7.5 | 11 | 1.04 | 51 | 0.42 | <2 | 14.6 | 41.4 | 339 |

| SAMPLE | Ni | Pb | Pr | Rb | Sm | Sn | Sr | Ta | Tb | Th | Tl | Tm | U | V | W | Y | Yb | Zn | Zr |
|--------|------|-----|-------|-----|-------|-----|-------|------|-------|-------|------|-------|-------|-----|-----|------|-------|-----|-----|
| Number | ppm | ppm | ppm | ppm | ppm | ppm | ppm | ppm | ppm | ppm | ppm | ppm | ppm | ppm | ppm | ppm | ppm | ppm | ppm |
| P.A1 | 152 | <5 | 3.85 | 3.2 | 4.07 | 2 | 531 | 0.5 | 0.67 | 2.15 | <0.5 | 0.32 | 0.54 | 215 | <1 | 22.1 | 2.01 | 90 | 82 |
| P.A2 | 193 | <5 | 3.7 | 2.2 | 3.89 | 1 | 707 | 0.4 | 0.63 | 2.03 | <0.5 | 0.3 | 0.5 | 210 | 2 | 21 | 1.9 | 80 | 77 |
| P.A4 | 1975 | <5 | <0.03 | 0.4 | <0.03 | <1 | 3.7 | <0.1 | 0.02 | <0.05 | <0.5 | 0.02 | <0.05 | <5 | 5 | <0.5 | <0.03 | 45 | <2 |
| P.A5 | 263 | <5 | 4.11 | 1.2 | 4.03 | 1 | 144.5 | 0.5 | 0.68 | 2.28 | <0.5 | 0.32 | 0.57 | 253 | 8 | 23.1 | 1.99 | 76 | 93 |
| P.A8 | 140 | 6 | 6.38 | 1.7 | 5.12 | 2 | 890 | 0.7 | 0.74 | 4.36 | <0.5 | 0.34 | 1.36 | 187 | 4 | 24.8 | 2.27 | 67 | 138 |
| P.A9 | 189 | <5 | 3.59 | 3.5 | 3.68 | 1 | 493 | 0.4 | 0.6 | 1.99 | <0.5 | 0.29 | 0.53 | 209 | 1 | 20.5 | 1.86 | 85 | 85 |
| P.A10 | 116 | <5 | 3.73 | 1.5 | 3.73 | 1 | 818 | 0.4 | 0.64 | 2.17 | <0.5 | 0.3 | 0.6 | 182 | 1 | 21.1 | 2.05 | 67 | 80 |
| P.A11 | 235 | <5 | 3.15 | 1.1 | 3.37 | 1 | 430 | 0.3 | 0.58 | 1.59 | <0.5 | 0.28 | 0.36 | 219 | 1 | 20 | 1.84 | 90 | 64 |
| P.A12 | 154 | <5 | 6.83 | 2 | 5.97 | 1 | 926 | 0.7 | 0.73 | 2.99 | <0.5 | 0.28 | 0.79 | 265 | 1 | 21.1 | 1.76 | 81 | 110 |
| P.A14 | 1865 | <5 | 0.17 | 0.4 | 0.09 | <1 | 34.2 | <0.1 | <0.01 | 0.14 | <0.5 | <0.01 | <0.05 | <5 | 1 | <0.5 | 0.03 | 37 | 7 |
| P.A15 | 36 | 7 | 2.29 | 1.7 | 2.85 | 1 | 806 | 0.1 | 0.49 | 2.28 | <0.5 | 0.24 | 0.61 | 312 | 1 | 16.1 | 1.49 | 39 | 82 |
| P.A16 | 204 | <5 | 5.59 | 0.9 | 4.13 | 1 | 1405 | 0.2 | 0.34 | 6.12 | <0.5 | 0.11 | 1.16 | 185 | 2 | 8.4 | 0.67 | 32 | 132 |
| P.A17 | 59 | 5 | 2.56 | 0.6 | 1.97 | <1 | 1530 | 0.1 | 0.27 | 3.07 | <0.5 | 0.13 | 0.34 | 140 | 1 | 8.6 | 0.84 | 27 | 90 |
| P.A20 | 339 | <5 | 11.1 | 0.7 | 8.48 | 2 | 183 | 1 | 0.97 | 18.15 | <0.5 | 0.4 | 2.08 | 257 | 3 | 28.5 | 2.6 | 57 | 448 |

Table-3: Continued

| SAMPLE | Eu/Eu* | Nb/Y | Zr/P ₂ O ₅ | Zr/Nb | La/Yb | (La/Yb) _N | Nd/Ce | Zr/Y | Zr/TiO ₂ | Na ₂ O+K ₂ O | La/Nb | (La/Sm) _N | Sm/Yb | Nb/Yb | Ba/Yb | Cr/Th | Th/La |
|--------|--------|------|----------------------------------|--------|--------|----------------------|-------|--------|---------------------|------------------------------------|-------|----------------------|-------|-------|--------|--------|-------|
| P.A1 | 0.606 | 0.33 | 0.05125 | 11.081 | 6.368 | 1.85 | 0.609 | 3.710 | 0.0066 | 5.12 | 1.73 | 1.92 | 2.02 | 3.68 | 37.21 | 134.88 | 0.17 |
| P.A2 | 0.602 | 0.33 | 0.03667 | 11.000 | 6.737 | 1.96 | 0.601 | 3.667 | 0.0068 | 4.91 | 1.83 | 2.05 | 2.05 | 3.68 | 33.00 | 187.19 | 0.16 |
| P.A4 | 1.567 | 0.40 | 0.01 | 10.000 | 16.667 | 5.2 | 0.200 | 4.000 | 0.0200 | 0.02 | 2.50 | 10.41 | 1.00 | 6.67 | 43.33 | 91200 | 0.10 |
| P.A5 | 0.734 | 0.36 | 0.02514 | 11.071 | 7.839 | 2.25 | 0.534 | 4.026 | 0.0079 | 3.19 | 1.86 | 2.42 | 2.03 | 4.22 | 14.62 | 271.93 | 0.15 |
| P.A8 | 0.936 | 0.49 | 0.069 | 11.311 | 11.322 | 2.28 | 0.495 | 5.565 | 0.0144 | 3.9 | 2.11 | 3.14 | 2.26 | 5.37 | 144.93 | 61.93 | 0.17 |
| P.A9 | 0.645 | 0.31 | 0.04722 | 13.281 | 7.258 | 3.302 | 0.521 | 4.146 | 0.0076 | 4.95 | 2.11 | 2.66 | 1.98 | 3.44 | 54.03 | 236.18 | 0.15 |
| P.A10 | 0.672 | 0.32 | 0.05 | 11.940 | 7.024 | 2.236 | 0.497 | 3.791 | 0.0069 | 5.27 | 2.15 | 2.419 | 1.82 | 3.27 | 31.02 | 133.64 | 0.15 |
| P.A11 | 0.672 | 0.25 | 0.04267 | 13.061 | 6.141 | 2.12 | 0.529 | 3.200 | 0.0063 | 4.25 | 2.31 | 2.101 | 1.83 | 2.66 | 29.84 | 345.91 | 0.14 |
| P.A12 | 0.597 | 0.58 | 0.03333 | 9.016 | 14.148 | 1.796 | 0.508 | 5.213 | 0.0076 | 4.24 | 2.04 | 2.605 | 3.39 | 6.93 | 51.88 | 137.12 | 0.12 |
| P.A14 | 0.673 | 0.40 | 0.07 | 35.000 | 30.000 | 4.124 | 0.429 | 14.000 | 0.0233 | 0.24 | 4.50 | 6.25 | 3.00 | 6.67 | 173.33 | 17214 | 0.16 |
| P.A15 | 0.723 | 0.12 | 0.11714 | 43.158 | 4.966 | 9.25 | 0.656 | 5.093 | 0.0128 | 7.16 | 3.89 | 1.62 | 1.91 | 1.28 | 189.93 | 57.02 | 0.31 |
| P.A16 | 0.515 | 0.44 | 0.066 | 35.676 | 31.642 | 1.45 | 0.517 | 15.714 | 0.0200 | 7.05 | 5.73 | 1.39 | 6.16 | 5.52 | 429.85 | 42.48 | 0.29 |
| P.A17 | 0.591 | 0.17 | 0.075 | 60.000 | 12.619 | 9.29 | 0.495 | 10.465 | 0.0191 | 8 | 7.07 | 3.366 | 2.35 | 1.79 | 0.8 | 65.15 | 0.29 |
| P.A20 | 0.562 | 0.51 | 0.15448 | 30.685 | 19.615 | 3.67 | 0.436 | 15.719 | 0.0339 | 3.59 | 0.16 | 3.79 | 0.02 | <0.01 | 1 | 49.59 | 0.36 |

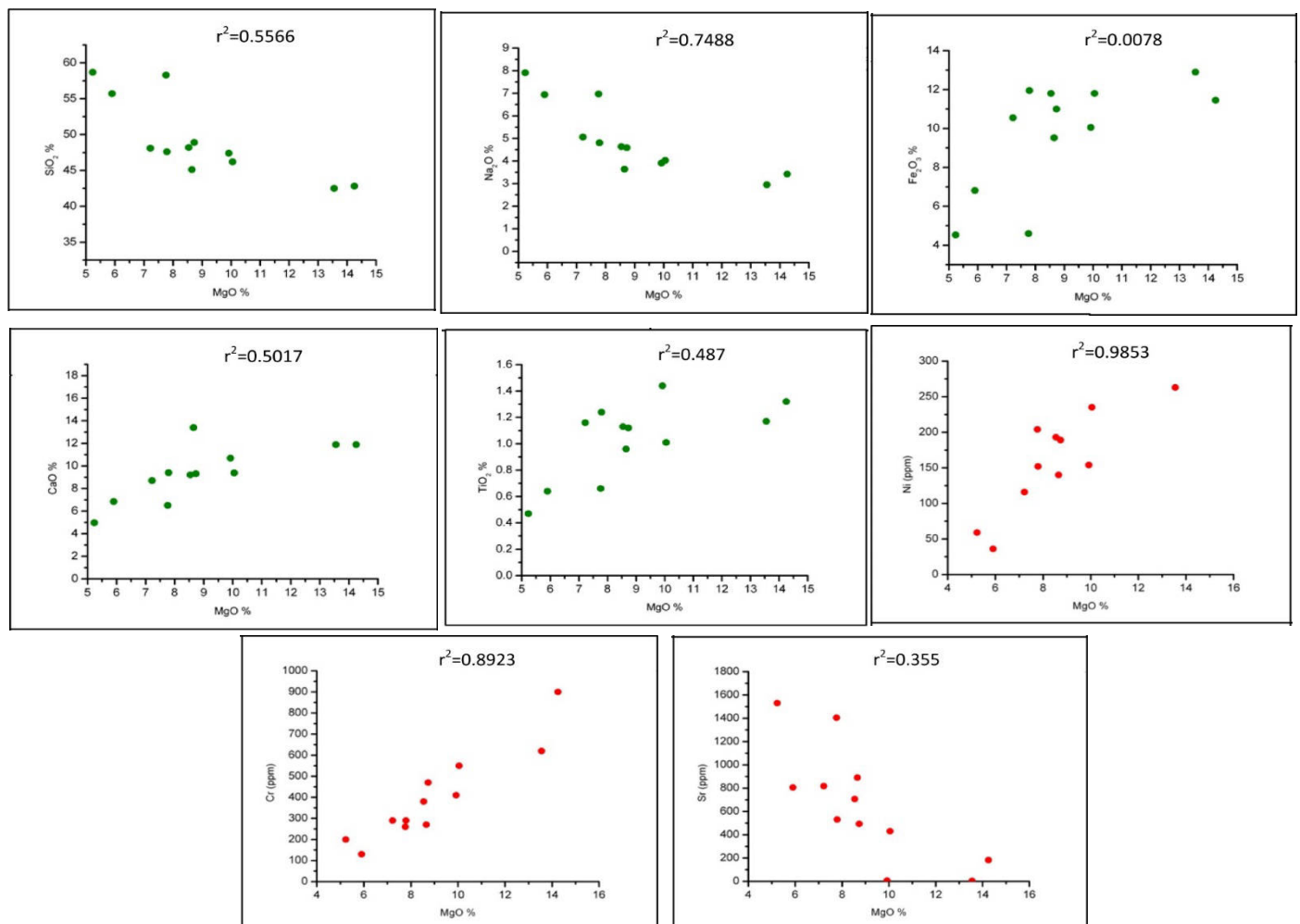


Figure 12: Harker variation diagrams for Penjween amphibolites showing the Trends of some major oxides and trace elements with MgO.

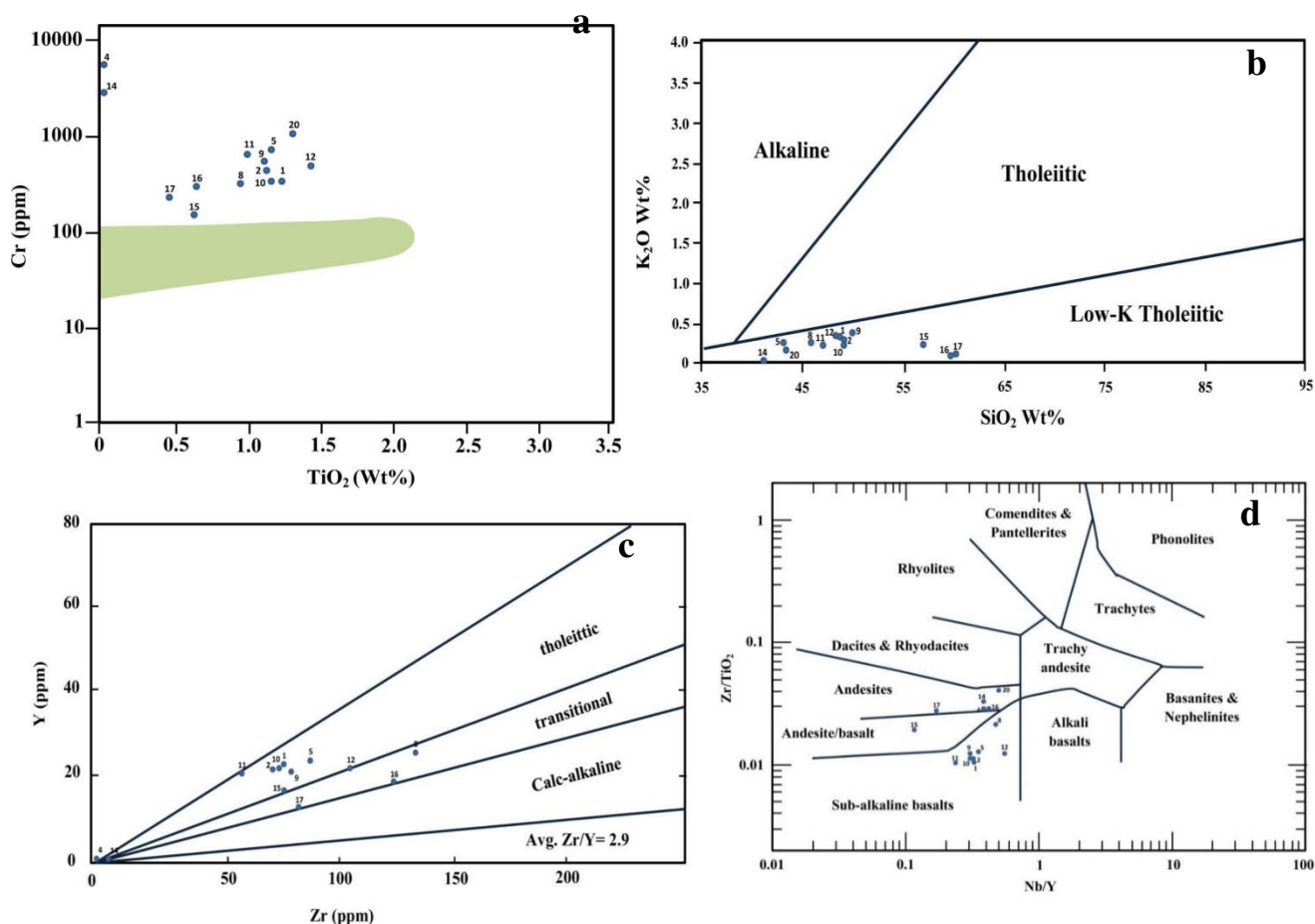


Figure 13: (a): Cr versus TiO₂ diagram for Penjween amphibolites. The shaded Area represents sedimentary protolith, the outside of the shaded Area represents igneous protolith. (after Leak,1964)

(b): K₂O versus SiO₂ diagram showing the plots of the amphibolites within Low-K tholeiite field, (after Peccerillo and Taylor, 1976).

(c): Zr versus Y diagram showing distribution of the amphibolites tholeiitic And transitional fields, (after Barret and Maclean,1999).

(d): Nb/Y versus Zr/TiO₂ diagram showing the possible protolith for amphi-bolites of Penjween ,(after Winchester and Floyd, 1977).

Chondrite-normalized REE patterns for Penjween amphibolites display a regular patterns (Fig.14-a) (normalization after Sun and McDonough, 1989). Such patterns imply a homogenous parental magma variously affected by partial melting and fractional crystallization (Pe-piper et al, 2004; El-Shazly and Hegaze, 2000). The concentration of REE varies in the range 10 and 100 × chon. with fractionated LREE relative to MREE and HREE (La/Sm)_N= 3.295, (La/Yb)_N= 3.917,(table-3), with pronounced positive Ce anomaly. Since Ce is incompatible with the major mantle mineral phases, this indicates its accommodation in the accessory minerals such as Fe-Ti oxides and also indicates the highly oxidizing condition environment. In addition, the decrease in abundance of TiO₂ with the increase of SiO₂ (table-3) and its increase with the increase of MgO and FeO confirm crystallization of titanomagnetite and high *f*O₂ in the melt as well as in the amphibole. Slight negative Eu anomaly is observed (Eu/Eu^{*}) = 0.859 avar.), (table-3), indicating plagioclase accumulation (Wilson,1989). Juster et al, (1989) and Patchett et al (1994) suggested that the lack of pronounced Eu anomaly may be explained due to fractionation in highly oxidation environment of Fe-Ti- rich magma with reduced $Kd_{Eu}^{plag-liquid}$. Furthermore,

the crystallization of calcic amphibole and clinopyroxene could effect on the Eu fractionation in plagioclase. More or less flat MREE is consistent with hornblende fractionation which may either be late magmatic as tschermakite or metamorphic as Mg-hornblende (Kocak et al, 2005). In general, the REE patterns of the amphibolites are indicative of island arc setting. The LREE/HREE ratios display a narrow variation consistent with the generation of magma by partial melting of mantle source in which garnet is residual phase (Wilson, 1989; Watson and McKenzie, 1991).

Primitive mantle- normalized trace elements diagram is relatively uniform (Fig.14-b), (normalization after Sun and Mc Donough, 1989) with striking variable concentrations of LILEs due to their mobilities and depletion of HFSEs and HREEs. Pronounced negative Nb and Ta anomalies which together with the positive Th anomaly reflect subduction-related environment nature of these amphibolites, specifically, a supra-subduction zone (SSZ) setting environment (Pearce,1982). Ba and Sr show great variability in their concentrations relative to the rest of the LILEs which could be due to their high mobility during metamorphism. On the other hand, Zr, Y and Yb are among the HFSE and HREE show negative anomalies in all samples reflecting their retentions in resistant minerals such as zircon, rutile, apatite, and sphene (titanite).

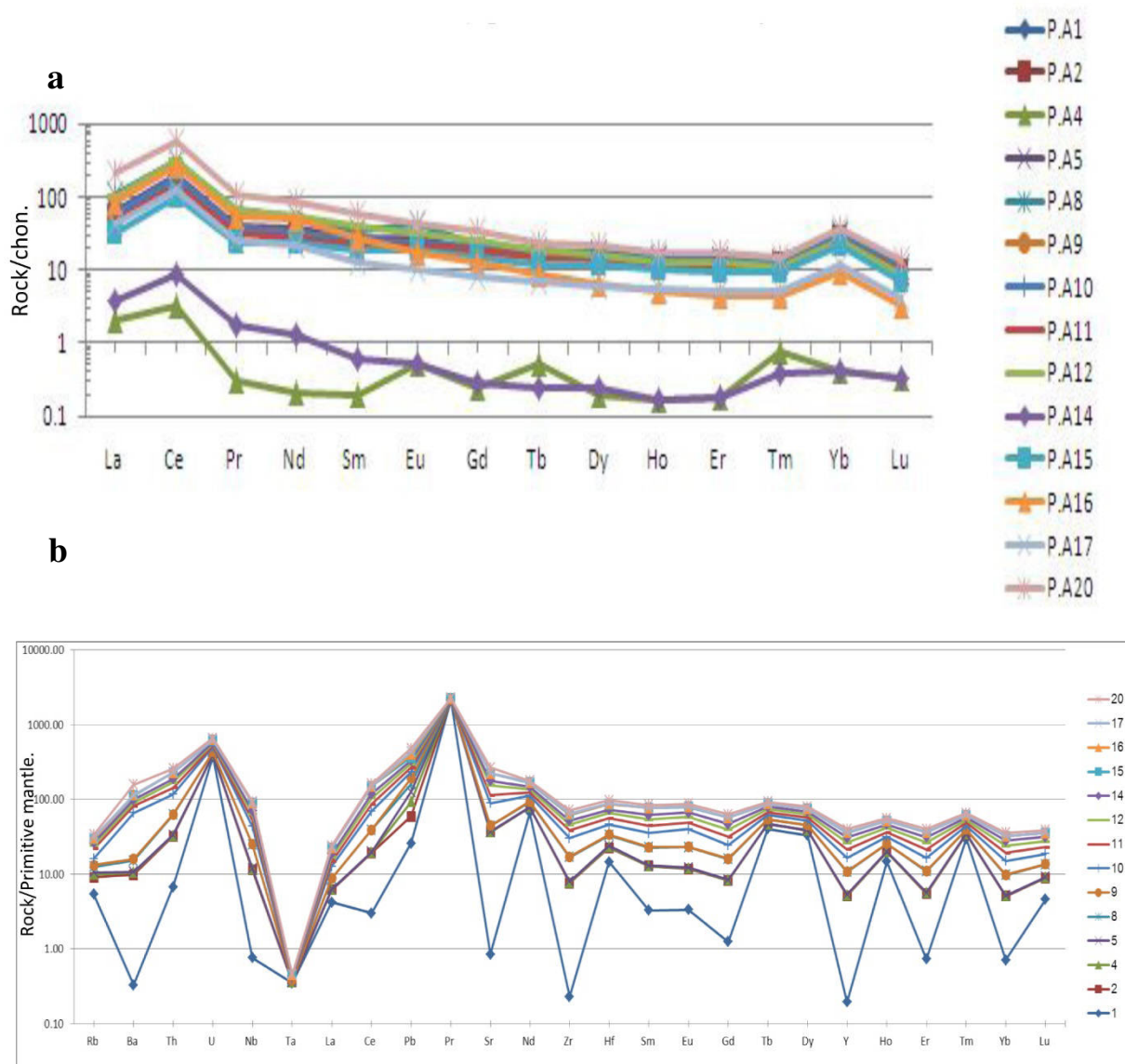


Figure 14: Chondrite-normalized REE patterns (a) and Primitive mantle-normal-ized spider diagrams (b) for Penjween amphibolites. Normalization Values for chondrite and primitive mantle are from Sun and McDonough, (1989).

7. Discussion

Based upon the geochemical data and observations previously described, the Penjween amphibolites have igneous protolith of tholeiitic basalt affinity. The paleotectonic setting and source magma as well as petrogenetic processes have been achieved using those elements that are considered to be immobile during alteration and metamorphism (e.g. Zr, Ti, Y and HREEs) on various discrimination diagrams. On La/Nb versus Nb/Th diagram, (Thompson et al, 1984), these amphibolites show the characteristic arc-setting environment (Fig.15-a). Both Th and Nb are incompatible elements that will be bound to the liquid fraction of the partially melting rocks; (Th) comes from the slab sediments and its content increases with increasing slab melting and dehydration in subduction zone (Pearce, 2008; Azizi et al, 2011), hence, Nb/Th ratio refers to the influence of subduction-related components. The low Ta content in regard to Th (table-3) coupled with the negative Ta and Nb anomalies (Fig.14-b) suggest mixing between IAT and MORB sources as in back-arc basin basalt (BABB). Y-La/Nb relationship (Fig.15b) is a good mean to illustrate the position of these amphibolites within BABB field with La/Nb ratio < 5 characteristic of BABB (Floyd et al, 1991) except two samples which were taken from amphibolite in contact with gabbro dyke. Thus a preliminary model for these amphibolites is proposed in which a back arc basin was developed on the continental crust at the leading edge of the plate which was subsequently invaded by tholeiitic magma due to subduction processes. The characteristics of the amphibolites can be better explained in terms of subduction input and mantle fertility. According to Sinton and Fryer (1987), Sinton et al (2003), and Pearce and Stern (2006), BABB setting is characterized by high subduction input (e.g. Ba, Sr,Th, etc) than MORB setting. The variations observed from plotting amphibolite data on Ba/Yb ratio (subduction input) versus Nb/Yb (mantle fertility) proposed by Pearce and Stern (2006) show their position within BABB with few within MORB array field with high Ba/Yb ratio values (Fig.16). The genesis of BABB magma could be related to supra-subduction of mantle and/or partial melting of shallow mantle by release of lithostatic pressure (Banerjee and Gills, 2001; Pearce, 2005; Kocak et al, 2007). LREE enrichment $(La/Yb)_N = 3.967$ is typical of metasomatized and metamorphosed mantle rocks by supra-subduction fluids enriched in LREEs from the fluids that accompanied subduction. For the estimation of source mantle composition and degree of partial melting, TiO_2 -Yb relationship is used (Fig.17 and 18). These amphibolites show low TiO_2 /Yb and Nb/Yb ratios content characteristic of BABB with the majority plotting within enriched mid-ocean basalt (EMORB) field since BABB setting is considered to be transitional between MORB and IAT settings (Sinton and Fryer, 1987). They show fractionation with 5-25 % partial melting within transitional zone between garnet lherzolite and spinel lherzolite but mostly closer to the former (Fig.18) which has estimated depth around 80 km (Wilson, 1989; Watson and McKenzie, 1991).

From field observation shows that the amphibolites of Penjween are directly related to the ultramafic rocks of Penjween ophiolite with sharp tectonic contact although they are observed in limited and discontinuous outcrops in the area. Geochemical characteristics and relationships as well as tectonic setting are all evidences that these amphibolites of tholeiitic nature of SSZ environment. They are similar to other metamorphic soles as in Turkey (Dilek et al,1999; Dilek,2003; Celik and Delayloye, 2003; Parlak et al, 2006). According to the obtained results and evidences we propose that during Late Cretaceous time the volcanic rocks and sea-floor sediments were detached and eventually emplaced by oceanic crust and upper mantle rocks that were then thrust over the northeastern margin of the Arabian Plate. Sufficient heat and pressure that accompanied the processes of detachment and emplacement could be enough to cause metamorphism at the base of the emplaced ultramafic rocks. Glent and Stout (1981) evaluated the possible P-T source of the metamorphic sole beneath Semail ophiolite of Oman and put an assumption that the dominant source P-T required for metamorphism is the residual heat and pressure from the ophiolite emplacement and that frictional heat during thrusting had a limited and minor effect. This dynamothermal sole beneath a supra-subduction-type ophiolite of Penjween could be explain by two stages of subduction; subduction of the southern branch of the Neo-Tethys oceanic crust beneath Iranian Plate during Late Cretaceous time followed by inception of a second subduction within a supra-subduction-type Penjween ophiolite. Wakebayshi and Dilek (2000) suggested that in a supra-subduction-type ophiolite-sole couples it is unlikely that the dynamothermal sole would be linked to the subduction that produced the overlying supra-subduction- type ophiolite and in such settings the metamorphic sole would be older than the ophiolite. Their conclusion appeared that the sole is younger. In the present study our conclusion based on the results of mineral chemistry and whole rock geochemical data. Precise age determination using radiometric dating as Ar^{40}/Ar^{39} for the amphibole is needed to clarify the age relationship between metamorphic sole-ophiolite as well as with the intrusive amphibole gabbro dyke.

The estimated temperature condition is high (550-900° C) coupled with medium to high pressure (1~2.5 GPa) within amphibolite facies grade, and such high grade metamorphic sole is probably compatible with subduction initiation within SSZ lithosphere protolith rather than MORB or OIB protoliths affinities which are characterized by high temperature-low pressure metamorphic grade (Wakabayashi et al,2010).

The occurrence of a late- stage gabbro dyke that cross-cut one of the amphibolite pods and the peridotite gives an inference that the basaltic magma was still available after the prograde metamorphism. Sharvaise (2001) assumed that such late-stage magmatism in a supra-subduction zone as dykes could be possibly originated from an asthenospheric window that underlies the displaced oceanic lithosphere in the upper plate as in Tauride ophiolite of Turkey (Dilek and Flower,2003), and Coast Range ophiolite of California (Sharvaise ,1990).

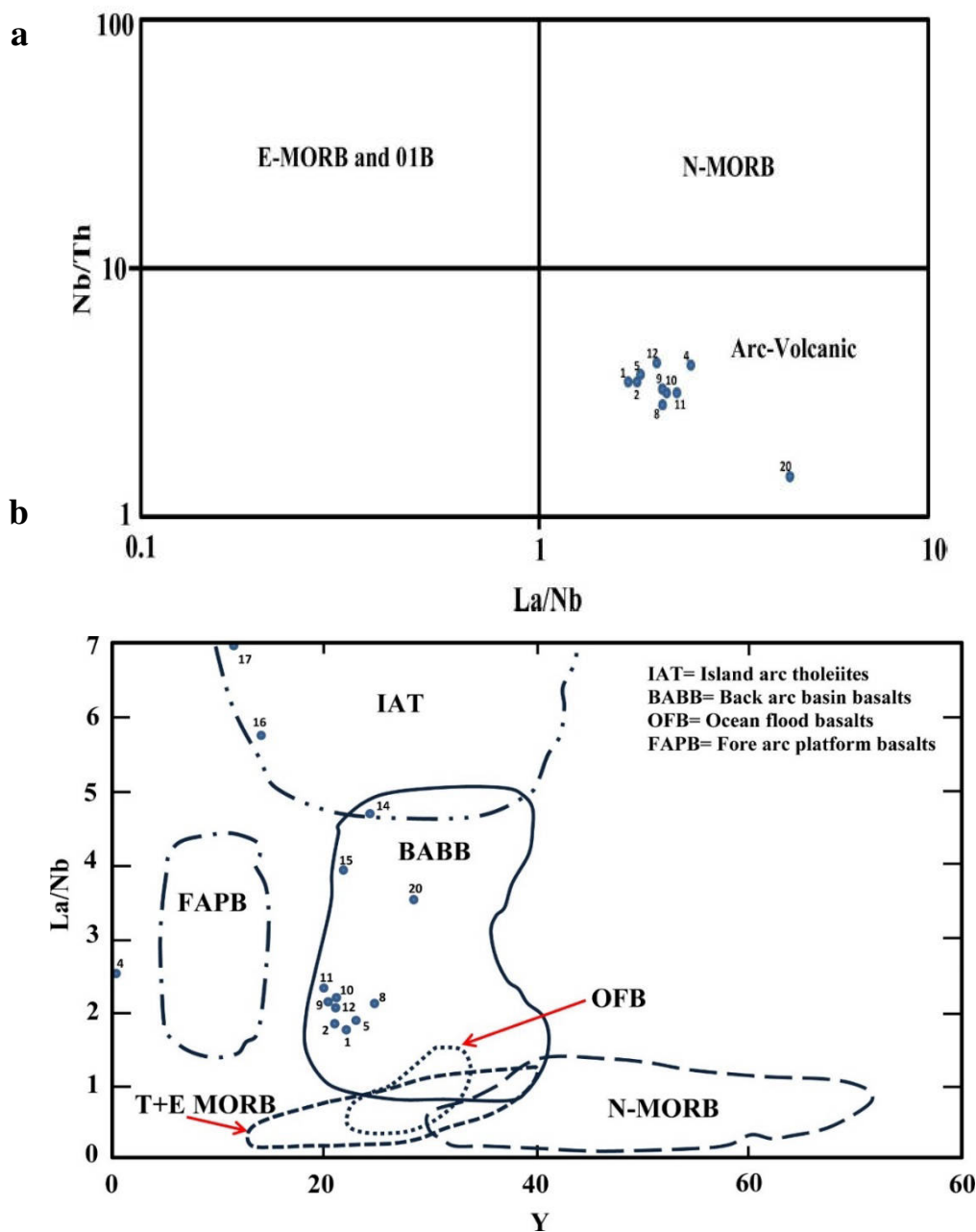


Figure 15: (a): La/Nb versus Nb/Th tectonic discrimination diagram showing the plots of the Penjween amphibolites within arc field,(after Thompson *et al* , 1984).

(b): Y versus La/Nb tectonic discrimination diagram showing the distribution of the majority of amphibolites within back-arc basin basalt (BABB) field, (after Floyd *et al* ,1991).

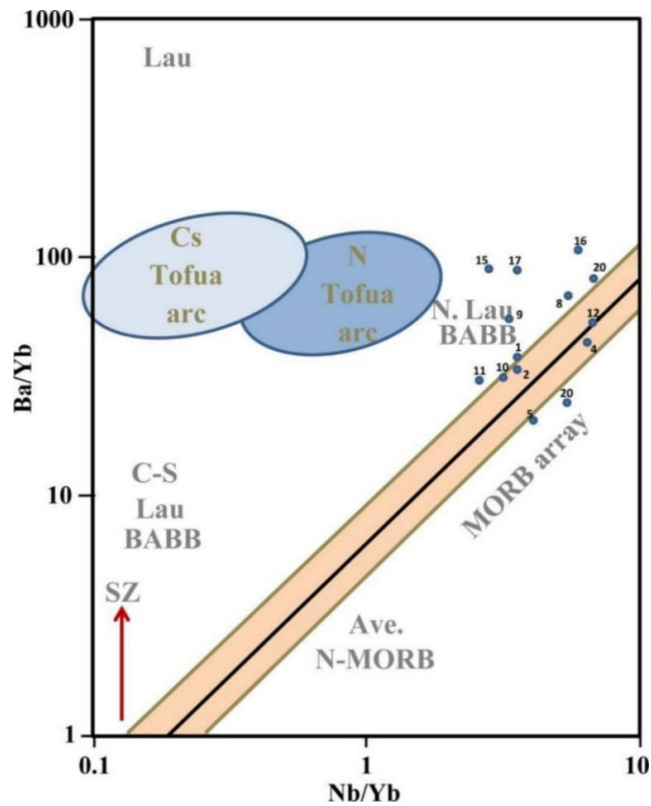


Figure 16: Nb/Yb versus Ba/Yb diagram showing the plots of the majority of amphibolites within BABB with few within MORB array,(after Pearce and Stern, 2006).

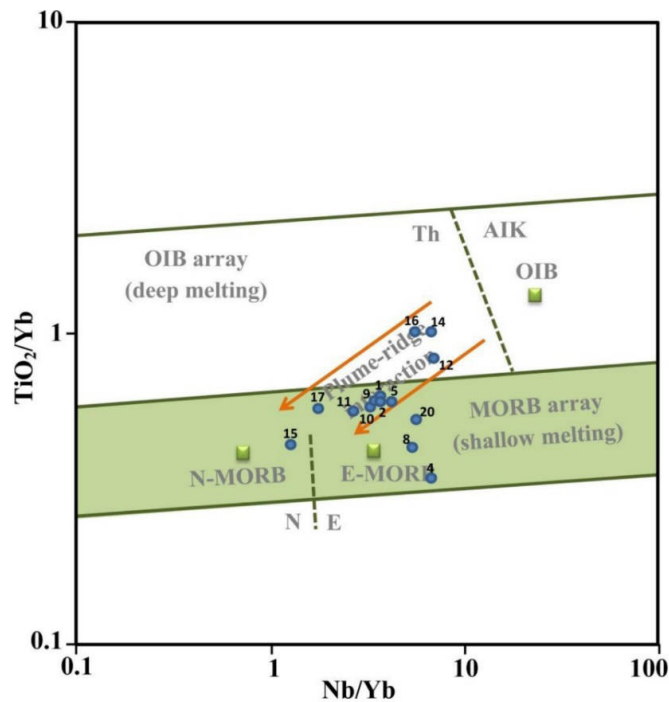


Figure 17: Nb/Yb versus TiO₂/Yb diagram (after Pearce,2008) showing the plots of the majority of the amphibolites within EMORB.

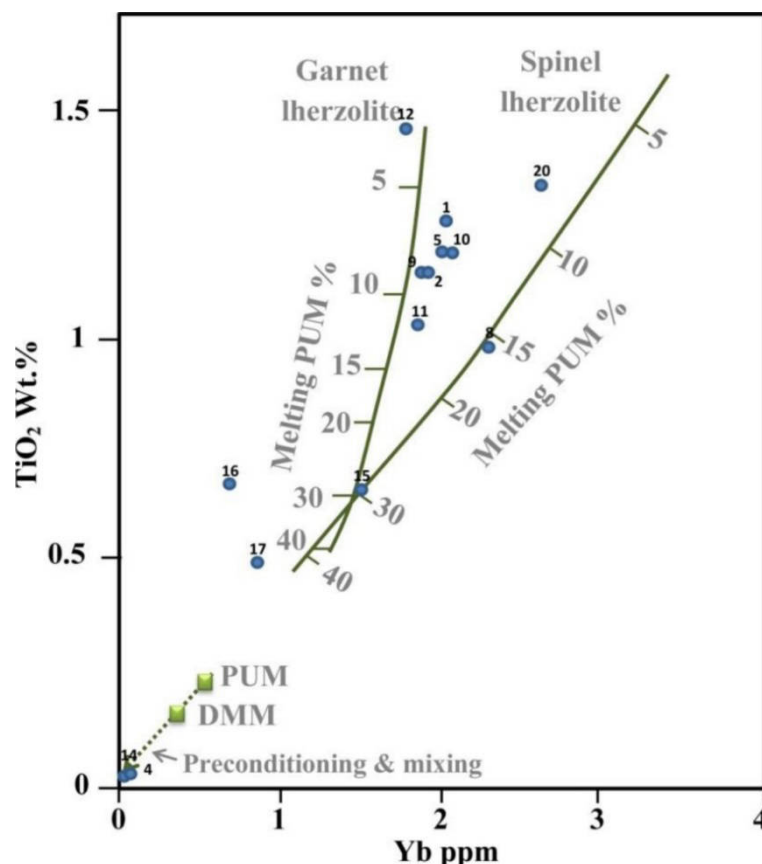


Figure 18: Yb versus TiO₂ diagram (after Pearce and Stern, 2006). The majority of amphibolite samples are clustered within the transitional field between garnet lherzolite and spinel lherzolite fields. PUM=primitive upper mantle, DMM= depleted MOR mantle

8. Conclusion

Amphibolite rocks in Penjween area is found to be related to ultramafic rocks; peridotite and serpentinized peridotite of the mantle succession of Penjween ophiolite complexe. The major mineral constituents in these amphibolites are amphibole and plagioclase with minor clinopyroxene , iron oxides and accessory quartz, titanite,apatite, and zircon. The amphiboles are calcic of two types; Mg-hornblende and tschermakite whereas the plagioclase ranges in composition between oligoclase and albite. P-T condition of metamorphism revealed that they are within amphibolite facies grade; P (1-2.5 GPa); T (550-850° C). The main textures are granoblastic, granonematoblastic, porphyroblastic, and poikiloblastic. Geochemical characteristics and relationships deduced their igneous origin with tholeiitic basalt affinity of sub-alkali basalt and andesite protolith. Primitive mantle-normalized trace element diagram, chond-normalized- REE patterns and tectonomagmatic discrimination diagrams revealed their arc and back-arc basin basalt settings of SSZ-type formed by two-stage subduction of the southern margin of the Neo-Tethys oceanic crust beneath the Iranian Plate in Late Cretaceous. Detachment and emplacement of the ophiolite rocks provided P-T condition for the formation of these amphibolites. Hence, based chiefly upon the intimate association of these amphibolites with the ultramafic rocks of Penjween ophiolite and upon their geochemical characteristics, we conclude that they represent the dynamothermal metamorphic sole of Penjween ophiolite.

Acknowledgment

The authors acknowledge the support of the Department of Earth Science, University of Baghdad for providing opportunity for this study. Special thanks go to Dr. Yawuz Kettaneh(University of Salahadeen,Erbil) for his valuable comments, Mr.Muhemmed Jameel (Department of Applied Geology, Kirkuk) for his help in field work.

References

- Agard, P., Omrani, J., Jolivet, L. and Mouthereau, F. (2005). Convergence history across Zagros (Iran): constraints from collisional and earlier deformation. *Int. Jour. Earth Sci.*, 94, 401-419.
- Alavi, M. (1994). Tectonics of the Zagros orogenic belt of Iran: new data and information. *Tectonophysics*, 229, 211-238.
- Alavi, M. (2004). Regional stratigraphy of the Zagros fold-thrust belt of Iran and its profore-land evolution. *Amer. Jour. of Sci.*, 304, 1-20.
- Al-Hassan, M.I. and Hubbard, F.H. (1985). Magma segregation in the tectonic remnant of basalt of ophiolite of Penjween, NE Iraq. *Ophioliti.*, 10, 139-146.
- Allahyari, K., Sc cani, E., Pourmoafi, M. and Beccaluva, L. (2010). Petrology of mantle peridotites and intrusive mafic rocks from the Kermanshah ophiolitic complex (Zagros belt, Iran): implication for the geodynamic evolution of the Neo-Tethyan oceanic branch between Arabia and Iran. *Ophioliti*, 35, 71-90.
- Aswad, K.J. (1991). Arc-continent collision in northeast Iraq as evidenced by the Mawat and Penjween ophiolite complexes. *Rafiden Jour. Sci.*, 10, 51-61.
- Azizi, H. and Jahangiri, A. (2008). Cretaceous subduction-related volcanism in the northern Sanadaj- Sirjan Zone, Iran. *Jour. of Geodynamics*, 45, 178-190.
- Azizi, H. and Moinevaziri, H. (2009). Review of the tectonic setting of Cretaceous to Quaternary volcanism in northeast Iran. *Jour. of Geodynamics*, 47, 167-179.
- Azizi, H., Asahara, Y., Mehrabi, B. and Lin Chung, S. (2011). Geochronological and geochemical constraints on the petrogenesis of high-K granite from Suffi Abad area, Sanandaj-Sirjan, NW Iran. *Chemie der Erde*, doi:10.1016/j.chemer.
- Banerjee, N.R. and Gills, K.M. (2001). Hydrothermal alteration in a modern supra-subduction Zone, the Tonga fore-arc. *Jour. Geoph. Res.*, 106, 21737-24750.
- Barrett, T.J. and Maclean, W.H. (1999). Volcanic sequences, litho-geochemistry, and hydrothermal alteration in some bimodal volcanic-associated massive sulfide system. In: Volcanic-associated massive sulfide system: Processes and examples in modern and ancient settings. C.T. and M.D. Hannington (eds.). *Rev. Econ. Geol.*, 8, 101-131.
- Berberian, M., and King, G.C.P. (1981). Toward paleogeography, and tectonic evolution of Iran. *Candian Jour. of Earth Sci.*, 18, 210-265.
- Buday, T. and Jassim, S.Z. (1987). The Regional Geology of Iraq, vol. 2: Tectonism, Magmatism and Metamorphism. *Geol. Min. Inv.*, Baghdad, 352 p.
- Celik, O.F. and Delaloye, M.F. (2006). Characteristics of ophiolite-related metamorphic rocks in Beysehir ophiolitic mélange (Central Taurides, Turkey) deduced from whole rock and mineral chemistry. *Jour. Asian Earth Sci.*, 26, 461-476.
- Deer, W.A., Howie, R.A., and Zussman, J. (1997). Rock-Forming Minerals. *Geol. Soc. Lond.*, U.K. Longman, 528 p.
- Dercourt, J., Zonenshian, L.P., Ricou, L.E., Kazmin, V.G. and Le Pichon X. et al (1986). Geological Evolution of the Tethys Belt from the Atlantic to the Pamirs since the Lias *Tectonophy.*, 123, 241-315.
- Dilek, Y., (2003), Ophiolite concept and its evolution, in Dilek, Y., and Newcomb, S, (eds.), Ophiolites Conceptand: The Evolution of Geological Thought. *Geol. Soc. Amer. Special Paper*, 373, 1-16.
- Dilek, Y., Thy, P., Hacker, B., Grundvig, S. (1999). Structure and petrology of Tauride ophiolites and mafic dike intrusions (Turkey): implications for the Neo-Tethyan Ocean. *Geol. Soc. Amer. Bull.*, 111, 1192-1216.
- Dilek, Y., and Flower, M.F.J., (2003). Arc-trench rollback and fore-arc accretion: 2. A model template for ophiolites in Albania, Cyprus, and Oman, in Dilek, Y., and Robinson, P.T. (eds.). Ophiolites in Earth History: *Geol. Soc. London Spec. Publ.* 218, 43-68.
- El-Shazly, S.M. and Hegazy, H.A. (2000). Geochemistry and Petrogenesis of Late Proterozoic volcanic sequences in Gabriel area, southeastern desert, Egypt. *Jour. of Sci. of Qatar University*, 20, 181-195.
- Ernst, W.G. and Liu, J. (1998). Experimental equilibrium study of Al and Ti content of calcic amphibole in MORB. A semi-quantitative thermobarometer. *Amer. Mineral.*, 83, 952-969.

- Floyd, P.A., Kelling, G. Gokcen, S.L., Gokcen, N. (1991). Geochemistry and tectonic environment of basaltic rocks from the Misis ophiolitic mélange, south Turkey. *Chem.Geol.*, 89, 263-380.
- Ghent, E.D. and Stout, M.Z. (1981). Metamorphism at the base of Semail ophiolite, southeastern Oman Mountain. *Jour. Geophys. Res.*, 86, *Spec. Issue*, 2552-2571.
- Jasmund, K. and Schafer, R. (1972). Experimental determination of P-T stability, its division in the mixed crystal series tremolite- tschermakite. *Contr. Mineral. Petrol.*, 34, 101-115.
- Jassim, S.Z. and Goff, J.C. (2006). *Geology of Iraq*. Dolin.Prague and Moravian Museum, 341p.
- Juster, T.P., Grove, T.L., Perfit, M.R. (1989). Experimental constraint on the generation of Fe- Ti –basalts, andesites, and rhodacite at Galapagos spreading center, 85° W and 95°W. *Jour. Geophys. Res.*, 94, 9251-9265.
- Kocak, K., Isik, F., Arslan, M., Zedef, V. (2005). Petrological and source region characteristics of ophiolitic hornblende gabbros from the Aksaray and Kayseri regions, Central Anatolian Crystalline Complex, Turkey. *Jour. Asian Earth Sci.*, 25, 883-891.
- Kocak, K., Kurt, H., Zedef, V., Ferré, E.C. (2007). Characteristics of the amphibolites from Nigde Metamorphics (Central Turkey), deduced from whole rock and mineral chemistry. *Geoch. Jour.*, 41, 241-257.
- Leak, B.E. (1964). The chemical distinction between ortho- and para-amphibolites. *Jour. Petrol.*, 5, 238-254.
- Leak, B.E., Woolley, A.R., Arps, C.E.S., Birch, W.D., Gilbert, M.C., Grice, J.D., Hawthorne, F.C., Kato, A., Kisch, H.J., Krivovichev, V.G., Linthout, K., Laird, J., Mandarino, J.A., Maresch, W.V., Nickel, E.H., Rock, N.M.S., Schumacher, J.C., Smith, D.C., Stephenson, N.C.N., Ungaretti, L., Whittaker, E.J.W., Youzhi, G. (1997). Nomenclature of Amphiboles: Report of the sub-committee on amphiboles of the international mineralogical association. Commission on new minerals and mineral names. *Amer. Mineral.*, 82, 1019-1037.
- Lippard, S.J., Shelton, A.W., Gass, I.G. (1986). The Ophiolite of Northern Oman. *Geol.Soc.London Mem.* 11, 178p.
- Mohammed, Y.O., Maekawa, H., Lawa, F. (2007). Mineralogy and origin of Malkawa albitite (Penjween) from Kurdistan region, northeast Iraq. *Geosphere*, 3, 624-645.
- Patchett, P.J., Lehnert, K., Rehkamper, M., Sieber, G. (1994). Mantle and crustal effects on the geochemistry of Proterozoic dykes and sills in Sweden. *Jour. Petrol.*, 35, 1095- 1125.
- Pearce, J.A., (1982). Trace element characteristics of lavas from destructive plate boundaries, in Thorpe, R.S., (ed.), *Orogenic Andesites*: Chichester, Wiley, 528–548.
- Pearce, J.A. (2005). Mantle preconditioning by melt extraction during flow: Theory and petrogenetic implications. *Jour. Petrol.*, *Doi: 10.1093/Petrol.legi007*.
- Pearce, J.A. (2008). Geochemical fingerprinting of oceanic basalts with applications to ophiolite classification and the search for Archean oceanic crust. *Lithos*, 100, 14-48.
- Pearce, J.A. and Stern, R.J. (2006). Origin of back-arc basin magmas: trace elements and isotope perspective. *Geophys. Monogr.*, 166, 63-86.
- Peccerillo, A., and Taylor, S.R. (1976). Geochemistry of Eocene calc-alkaline volcanic rocks from the Kastamonu area, northern Turkey. *Contrib. Mineral. Petrol.*, 58, 81-93.
- Pe-Piper, G., Tsikouras, B., Hatz, K. (2004). Evolution of boninitic and island arc tholeiites in the Pindos ophiolite, Greece. *Geol. Mag.*, 141, 455-469.
- Parlak, O., Yilmaz, H., and Boztug, D., (2006). Origin and tectonic significance of the metamorphic sole and isolated dykes of the Divrigi ophiolite (Sivas, Turkey): Evidence for slab break-off prior to ophiolite emplacement. *Turkish Jour. of Earth Sci.*, 15, 25–45.
- Raase, P. (1974). Al and Ti contents of hornblende, indicators of pressure-temperature of regional metamorphism. *Contr. Mineral. Petrol.*, 45, 231-236.
- Raase, P., Raith, M., Ackermann, D., Lal, R.K. (1986). Progressive metamorphism of mafic rocks from greenschist to granulite facies in the Dharwar Craton of South India. *Jour. Geol.* 94, 261-282.
- Ricou, L.E., Braud, J., Brunn, J.A. (1977). Le Zagros: Mémoire Societe Géologique de France: *Hors-Série*, 8, 33-52.

Rollinson, H. (1996). Using geochemical data: Evaluation, Presentation, Interpretation. Longman Ltd. Essex, England, 352p.

Shervais, J.W., (1990). Island arc and ocean crust ophiolites; contrasts in the petrology, geochemistry and tectonic style of ophiolite assemblages in the California Coast Ranges, *in* Malpas, J., Moores, E., Panayiotou, A. and Xenophontos, C. (eds): Ophiolite oceanic crustal analogues: Proceedings of the Symposium "Troodos 1987": Nicosia, Cyprus, Geological Survey Department, Ministry of Agriculture and Natural Resources, 507–520.

Shervais, J.W., (2001), Birth, death, and resurrection: The life cycle of supra-subduction zone-ophiolites: Geochemistry, Geophysics, Geosystem (2001), *doi:10.1029/2000GC000080*.

Sinton, J.M., and Fryer, P. (1987). Mariana trough from 18°N: Implication for the origin of back-arc basin basalts. *Jour. Geophys. Res.*, 92, 12782-12802.

Sinton, J.M., Ford, L.L., Mc Culloch, M.T., (2003). Magma genesis and mantle heterogeneity in Manus back-arc basin, Papua, New Guinea. *Jour. of Petrol.*, 44, 159-195.

Stampfli, G., Mosar, J, Faure, P., Pillecuit, A. Vannay, J.C. (2001). Permo-Mesozoic evolution of the western Tethys realm: The Neo-Tethys East mediterranean basin connection, *in*: P. Ziegler, W. Cacazza, A.H.f. Robertson and S. Crasquin- Soleau (eds), Peri-Tethyan rift/wrench basins and passive margins. *Mem. Mus. Nat., Peri-Tethys Mem.*, 5, 51-108.

Stöckline, J. (1968). Structural history and tectonics of Iran: a review. *Bull. Amer. Assoc. Petrol. Geol.*, 52, 1229-1258.

Sun, S. and McDonough, W.F. (1989). Chemical and isotopic-systematics of oceanic basalts: Implications for mantle composition and processes, *in*: A.D. Saunders and M.J. Norry (eds): Magmatism in the ocean basins. *Geol. Soc. London. Spec. Publ.*, 42, 313-345.

Takanobu, O. (1978). Phase relationship of $\text{Ca}_2\text{Mg}_3\text{Al}_2\text{Si}_6\text{Al}_2\text{O}_{22}(\text{OH})_2$ - $\text{Ca}_2\text{Mg}_3\text{Fe}_2\text{Si}_6\text{Al}_2\text{O}_{22}(\text{OH})_2$ join at high temperature and high pressure. The stability of tschermakite. *Jour. Fac. Soc., Hokkaido Univ., Ser. IV*, 18, 339-350.

Takin, M. (1972). Iranian geology and continental drift in the Middle East. *Nature*, 23, 147- 150.

Taylor, S.R. and McLennan, S.M. (1985). The Continental Crust: Its Composition and Evolution. *Blackwell, London*, 312p.

Thompson, R.N., Morrison, M.A., Hendry, G.L., Parry, S.J. (1984). An assessment of the relative roles of the crust and mantle in magma genesis, an elemental approach. *Philp. Trans Royal Soc. London*, 310, 549-590.

Wakabayashi, J., and Dilek, Y., (2000). Spatial and temporal relations between ophiolites and their sub-ophiolitic soles: A test of models of fore-arc ophiolite genesis, *in* Dilek, Y., Moores, E.M., Elthon, D., and Nicolas, A., (eds), Ophiolites and Oceanic Crust :New Insights from Field Studies and Ocean Drilling: *Geol.Soc.Amer.Spec.Paper*, 349, 53–64.

Wakabayashi, J., Ghatak, A., Basu, A.R. (2010). Supra-subduction zone ophiolite generation, emplacement, and initiation of subduction. A perspective from geochemistry, metamorphism, geochronology and regional geology. *Geol. Soc. Amer.*, 122, 1548-1568.

Wilson, M. (1989). Igneous Petrogenesis. Unwin-Hyman, London, 456p.

Winchester, J.A. and Floyd, P.A. (1977). Geochemical discrimination of different magma series and their differentiation products using immobile elements. *Chem. Geol.*, 20, 325- 343.

This academic article was published by The International Institute for Science, Technology and Education (IISTE). The IISTE is a pioneer in the Open Access Publishing service based in the U.S. and Europe. The aim of the institute is Accelerating Global Knowledge Sharing.

More information about the publisher can be found in the IISTE's homepage:

<http://www.iiste.org>

CALL FOR JOURNAL PAPERS

The IISTE is currently hosting more than 30 peer-reviewed academic journals and collaborating with academic institutions around the world. There's no deadline for submission. **Prospective authors of IISTE journals can find the submission instruction on the following page:** <http://www.iiste.org/journals/> The IISTE editorial team promises to review and publish all the qualified submissions in a **fast** manner. All the journals articles are available online to the readers all over the world without financial, legal, or technical barriers other than those inseparable from gaining access to the internet itself. Printed version of the journals is also available upon request of readers and authors.

MORE RESOURCES

Book publication information: <http://www.iiste.org/book/>

Recent conferences: <http://www.iiste.org/conference/>

IISTE Knowledge Sharing Partners

EBSCO, Index Copernicus, Ulrich's Periodicals Directory, JournalTOCS, PKP Open Archives Harvester, Bielefeld Academic Search Engine, Elektronische Zeitschriftenbibliothek EZB, Open J-Gate, OCLC WorldCat, Universe Digital Library, NewJour, Google Scholar

